http://ijopaar.com; 2017 Vol. 1(1); pp. 07-41.

Conformational stability, spectroscopic (FT-IR, FT-Raman) analysis, fukui function, Hirshfeld surface and docking analysis of Naphthalene-2-lyoxy acetic acid by density functional theory

M. Kavimani[1], V. Balachandran[1], B. Narayana[2], K. Vanasundari[1]

[1]Centre for Research-Department of Physics, Arignar Anna Govt. Arts College, Musiri, Tiruchirappalli 621211, India.
[2]Department of Studies in Chemistry, Mangalore University, Mangalagangotri 574 199, India
Email: brsbala@rediffmail.com

Date of revised paper submission: 03/02/2017; Date of acceptance: 15/03/2017
Date of publication: 25/03/2017; *First Author / Corresponding Author; Paper ID: B17102.
Reviewers: Awasthi, D. K., India; Soni, A.K., India.

Abstract

The experimental and theoretical study on the structure and vibrations of Naphthalene-2-lyoxy acetic acid (NLA) are presented. The FT-IR and FT-Raman spectra of the title compound have been recorded in the region 4000-0 cm^{-1} and 3500-100 cm^{-1}. The molecular structure, vibrational wave numbers infrared intensities and Raman intensities were calculated using DFT (B3LYP) method with LANL2DZ and LANL2MB basis sets. The conformational behavior of the molecule was also investigated. The vibrational wave numbers were calculated using DFT quantum chemical calculations. The data obtained from the wave number calculations are used to assign vibrational bands obtained through an experiment. The stability of the molecule arising from charge delocalization and hyper-conjugative interaction has been analyzed by NBO analysis. The HOMO and LUMO analysis were used to verify the charge transfer at intervals the molecule and quantum chemical parameters connected to the title compound. From the MEP analysis, it is clear that the ring and are possible sited for electrophilic attack and the positive regions are localized at all the hydrogen atoms as possible sites for nucleophilic attack. Fukui function and Mulliken analysis on atomic charges of the title compound have been discussed. The Hirshfeld surface analysis and fingerprint plots are reported the title molecule and reveal that the structures are stabilized intermolecular interactions. It is clear from the docking studies that NLA has inhibition capability toward the plant growth protein target 4Y31, 4PSB and 4QOK.

Keywords: Vibrational spectra; HOMO-LUMO; MEP; NBO; Hirshfeld; Docking.

1. Introduction

Acetic acid cyclohexyl organic compound, by-product of acetic acid, may be a colourless liquid with characteristic odour. Its boiling point is 177°C. It is immiscible in water and soluble in alcohol however insoluble in water and combustible. Besides, it reacts with strong oxidants inflicting fire and explosion hazard. Acetic acid cyclohexyl estier are utilized in large quantities as solvents for plastics, lacquers, resins and gums. It's used as solvent for nitrocellulose, polyose ether, bitumen's, metallic soaps, basic dyes, blown oils, crude rubber, several natural and artificial resins, gums and lacquers. And therefore the Naphthalene provides the most effective material for the preparation of NLA that may be a terribly stable fused cyclic with a great deal of aromatic character. Aromatic rings

give the frame work for mony of dyes. Dyes owe their color to the functional groups present in them, and particularly Naphthalene plays important role during this field. Naphthalene is additionally a valuable pestiside. The major industrial use of Naphthalene is within the manufacture of polyvinyl chloride (PVC) plastics. Its major client uses are mouth repellents and toilet deodorant blocks and for creating different chemicals and resins. Supported the results from animal studies the U.S Department of Health and Human Services (DHHS) has all over that Naphthalene are often moderately expected to be a human carcinogen [1]. This was also confirmed by the "Internet Agency of Research of Cancer (IARC) and the Environmental Protection Agency (EPA). Exposure to large amounts of Naphthalene might damage or destroy some red blood cells, resulting in a condition referred to as hemolytic anemia. NLA may be an artificial phytohormone within the auxin family and is an ingredient in several commercial plants rooting horticultural products; it's a rooting agent and used for the Vegetative propagation of plants from stem and leaf cutting. It is also used for plant tissue culture. The hormone NLA doesn't occur naturally and like all auxins, is toxicant to plants at high concentrations [2]. Within the United States, beneath the Federal pesticide, antimycotic agent and Rodenticide Act (FIFRA), merchandise containing NLA require registration with the Environmental Protection Agency (EPA) as pesticides.

Due to the great biochemical importance the vibrational spectral studies of NLA are carried out in the present investigation. Various possible conformers were tried for the energy calculations at LANL2DZ and LANL2MB basis sets. The foremost optimized geometry (global minimum energy) obtained for NLA was used for the density functional theory calculations supported B3LYP functional with these basis sets. The IR and Raman intensities were additionally predicated theoretically. That supported simulated IR and Raman spectra were obtained additionally. The observed and the simulated spectra agree well. The energies, hybridization, populations of the lone pairs of oxygen, hydrogen atoms, energies of their interaction with the anti bonding orbital of the benzene ring and therefore the electron density distributions and E(2) energies are calculated by NBO analysis using DFT method. It's providing to the clear proof of stabilization originating from the hyper-conjugation of different intra-molecular interactions. There has been growing interest in using organic materials for nonlinear optical devices, functioning as SHG (second harmonic generations), frequency converters, EOM (electro optical modulators) etc., attributable to the high second order electric susceptibility is related to first hyperpolarizability, explore for organic chromophores with large first hperpolarizability was totally justified. Moreover, Mulliken population analysis and calculated values of Fukui function using the Mulliken charges.

2. Experimental details

(Naphthalene-2-lyoxy) acetic acid (C12H9O3) was used in and of itself without any more purification. The room temperature Fourier transform infrared spectrum of NLA was measured within the region 4000-400 cm^{-1} at a resolution of ± 1 cm^{-1} using a BRUKER IFS-66V FT-IR spectrometer equipped with a cooled MCT detector for the Mid-IR range, KBr pellet were utilized in the spectral measurements. The FT-Raman spectrum of NLA was recorded on a BRUKER IFS-66V model interferometer equipped with on FRA-106 FT-Raman accent at on intervals the region 3500-100 cm^{-1} using the 1064 nm line of a Nd:YAG laser for excitation operational at 200 mW power. The according frequencies are expected to be accurate among $\pm 1 cm^{-1}$.

3. Computational details

Calculations of the title compound were dispensed with Gaussian09 program using the DFT/B3LYP (Becke3-Lee-Yang-Parr with LANL2DZ and LAN2DMB basis sets to predict the

molecular structure and vibrational wave numbers. Molecular geometry was totally optimized by Berny's optimization algorithmic rule using redundant internal coordinates. Harmonic vibrational wave numbers has been calculated using the analytic second derivatives to verify the convergence to minima on the potential surface. The DFT hybrid B3LYP functional method tends to overestimate the fundamental modes. Therefore the scaling factor of 0.9631 must be used [3] for obtaininig a significantly agreement with the experimental data. The absence of imagined wave numbers on the calculated vibrational spectrum confirms that the structure deduced corresponds to lower energy. The assignments of the calculated wave numbers are power assisted by the animation possibility of GAUSSVIEW program, which provides a visible presentation of the vibrational modes. The potential energy distribution (PED) is calculated with the assistance of Computer with the version V7.0-G77 of the MOLVIB program written by sundius [4,5] .

4. **Prediction of Raman intensities**

The Raman intensities (I_i) were calculated from the Raman activities (S_i) obtained with the Gaussian 09 program, using the subsequent relationship derived from the intensity theory of Raman scattering [6].

$$I_i = \frac{f(\nu_0 - \nu_i)^4 \, S_i}{\nu_i[1 - \exp(-hc\nu_i)]kT}$$

Wherever ν_0 is the exciting frequency (in cm^{-1} units), ν_i is that the vibrational frequency if the i^{th} traditional mode, h, c and k are the universal constants and f is the appropriately chosen common scaling factor for all the highest intensities. The simulated IR and Raman spectra are planned using Lorentzian band shapes with FWHM bandwidth of 10 cm^{-1}.

5. Potential Energy Distribution:

A normalized potential energy distribution are often expressed as

$$PED = \frac{F_{ii} L_{ik}^2}{\lambda_k}$$

wherever $\mathbf{F_{ii}}$ are the force constants outlined by damped least square technique, $\mathbf{L_{ik}}$ the normalized amplitude of the associated element (i,k) and λ_k the eigen value such as the vibrational frequency of the element k. The PED contribution corresponding to the energy of the observed frequencies over 10% are alone listed in the present work.

6. Results and Discussion

In order to find the foremost optimized geometry, the energy calculations were dispensed out for various possible conformers. The varied possible conformers of NLA are shown in Fig.1. For NLA, the global minimum energy calculations were distributed using B3LYP/LANL2DZ and LANL2MB for 8 whole completely different possible conformers. The total energies obtained for the 8 conformers are presented in Table.1. It's clear from Table 1 that the conformer C8 has produced the global energy minimum. The numbering of the most stable conformer and therefore the crystal packing structure for the title compound are shown in Figs. 2(a) and 2(b) respectively.

From the structural purpose of reading of the molecule belongs to C1 point group symmetry. The 25 atoms with 69 fundamental modes of vibrations are same symmetry species. The optimized geometrical parameters such as bond length, bond angles and dihedral angles were calculated by

B3LYP with the basis sets LANL2DZ and LANL2MB were presented in Table 2. The compared optimized geometries for each the basis sets were pasteurized in Figs. 3-5.

7. Vibrational assignments

Comparison of the frequencies calculated at B3LYP with experimental values reveals the overestimation of the calculated vibrational modes as a result of the neglect of anharmonicity in a real system. Anyway, notwithstanding the extent of calculations, it is customary to scale down the calculated harmonic frequencies. In our study, vibrational frequencies calculated at B3LYP/LANL2DZ and B3LYP/LANL2MB levels were scaled by 0.9574 and 0.9631, sevarally [7].

After scaled with a scaling factor, the deviation from experiments is less than 10 cm^{-1} with many exceptions. The vibrational band assignments are created by using both the animation option of GAUSSVIEW 5.0 graphical interface for Gaussian programs [8] and version V7.0-G77 of the MOLVIB program written by Sundius [9]. The B3LYP/LANL2DZ level of theory is superior to B3LYP/LANL2MB in terms of a realistic copy of each band intensity distribution and general spectral features. The harmonic vibrational frequencies (scaled) calculated at LANL2DZ and LANL2MB basis set, determined FT-IR, FT-Raman frequencies, IR and Raman activity for various modes of vibrations are listed in Table.3. The observed and simulated FT-IR and FT-Raman spectra of the title compound are shown in Figs.6 and 7 respectively.

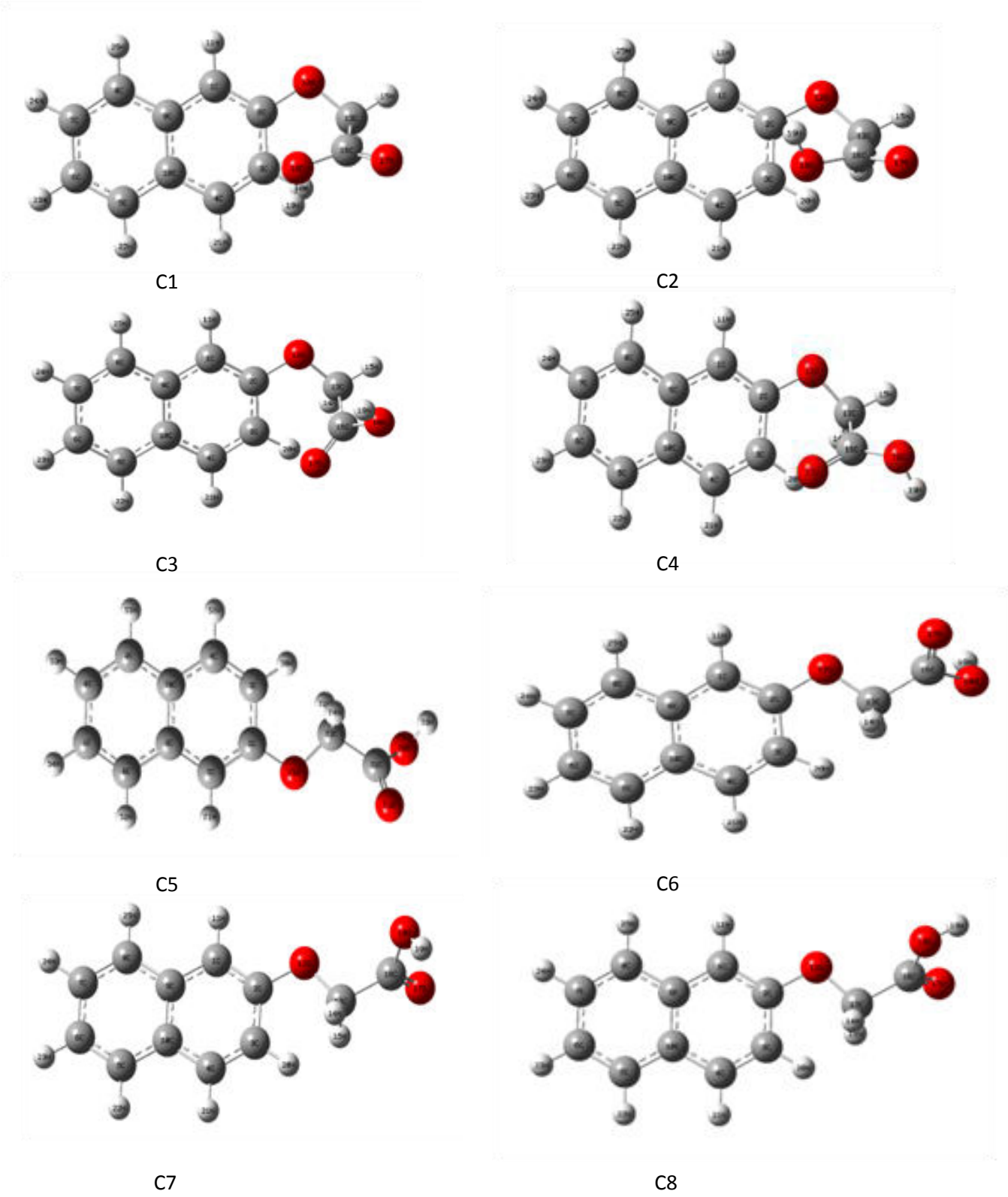

Fig. 1 Various possible conformers of Naphthalene-2-lyoxy acetic acid.

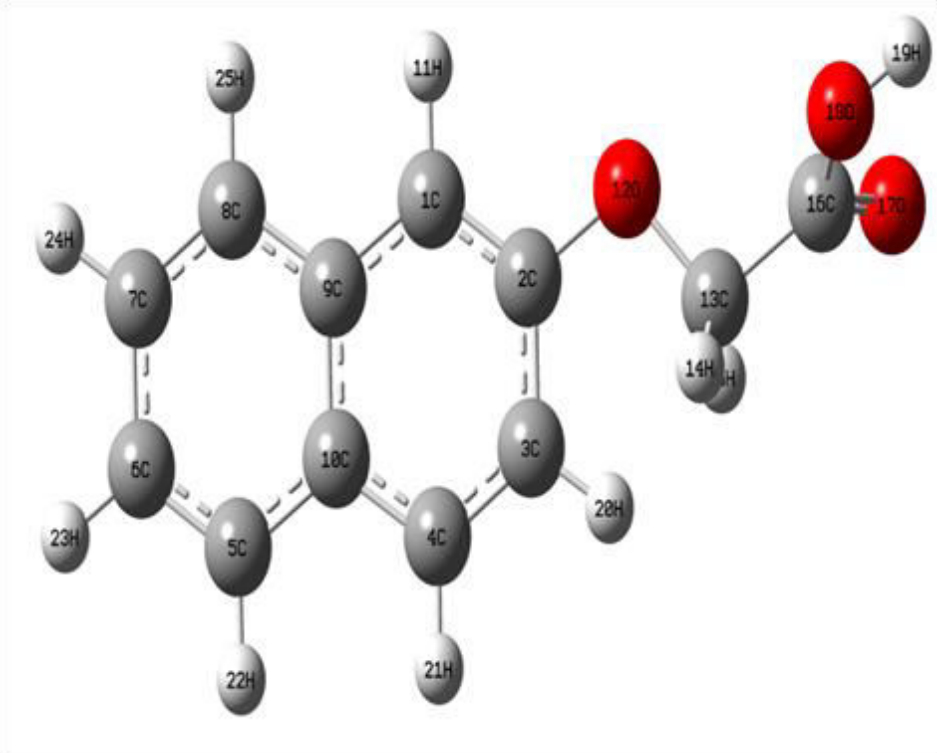

Fig. 2a Stable conformer structure of Naphthalene-2-lyoxy acetic acid.

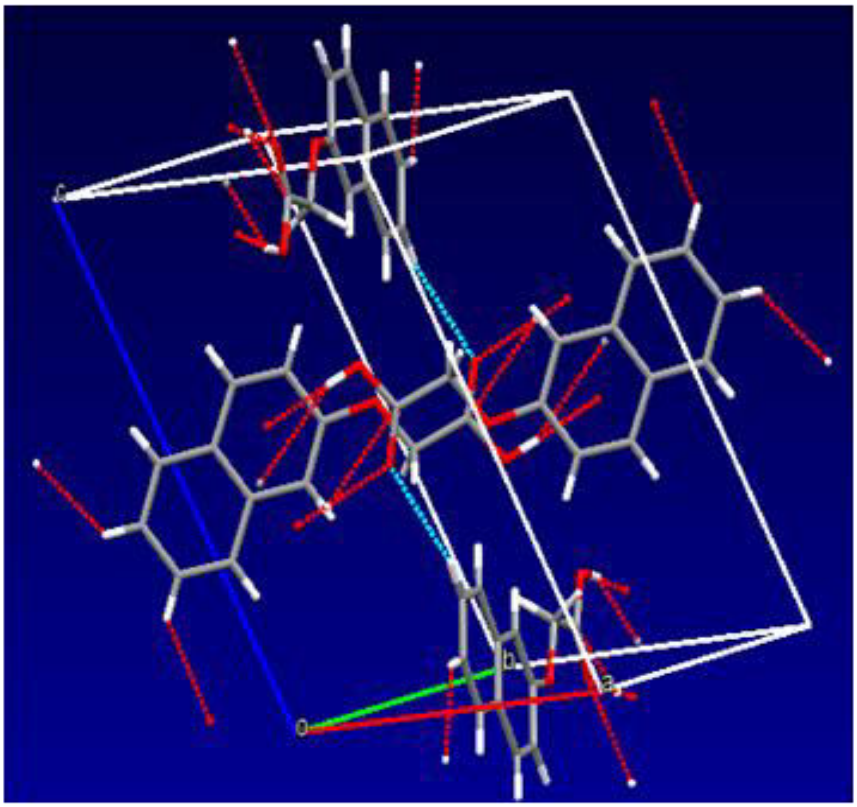

Fig. 2 b Crystal Packing Structure for Naphthalene-2-yloxy acetic acid

Table 1

Total energies (B3LYP) and kJ/mol of different conformations of Naphbthalene-2-yloxy Acetic Acid calculated at the B3LYP/LANLDZ and B3LYP/LANL2MB level of theory

Conformers	Energies a.u		Energies (kJ mol^{-1})		Energy difference (kJmol^{-1})	
	B3LYP/LANL2DZ	B3LYP/LANL2MB	B3LYP/LANL2DZ	B3LYP/LANL2MB	B3LYP/LANL2DZ	B3LYP/LANL2MB
C1	-688.74596637	-680.04590100	-1808302.6724536	-1785460.6490847		
C2	-688.76702298	-680.06449995	-1808357.9565874	-1785509.4806316	+55.2841338	+48.8315469
C3	-688.74659074	-680.04464773	-1808304.3117372	-1785457.358624	-53.6448502	-52.1220096
C4	-688.73966450	-680.03971288	-1808286.1268927	-1785444.4021744	-18.1848445	-12.9564496
C5	-688.83119313	-680.11110514	-1808526.4353291	-1785631.8425673	+240.3084364	+187.4403929
C6	-688.83743810	-680.11159621	-1808542.8314990	-1785633.1318717	+16.3961699	+1.2893044
C7	-688.83209398	-680.11167824	-1808528.8005109	-1785633.3472415	-14.0309881	+0.21253698
C8	-688.85229716	-680.13152223	-1808581.843964	-1785685.4476412	+53.0434531	+52.1003997

Table 2

Optimized geometrical parameters of (Napthalen-2-lyosy) acetic acid obtained B3LYP/ lanl2dz and B3LYP/ Lanl2mp density functional calculations:

Bond length(Å)			Bond angle(degree)			Dihedral angle (degree)		
Parameters	LANL2DZ	LANL2MB	Parameters	LANL2DZ	LANL2MB	Parameters	LANL2DZ	LANL2MB
C_1-C_2	1.39	1.4	C_2-C_1-C_9	120.45	120.65	C_9-C_1-C_2-C_3	0.06	-0.89
C_1-C_9	1.42	1.43	C_2-C_1-H_{11}	118.97	119.5	C_9-C_1-C_2-O_{12}	179.32	-178.52
C_1-H_{11}	1.09	1.1	C_9-C_1-H_{11}	120.58	119.86	H_{11}-C_1-C_2-C_3	179.86	179.44
C_2-C_3	1.43	1.44	C_1-C_2-C_3	120.87	120.38	H_{11}-C_1-C_2-O_{12}	-0.88	1.82
C_2-O_{12}	1.41	1.43	C_1-C_2-C_{12}	115.62	115.16	C_2-C_1-C_9-C_8	179.91	-179.63

C_3-C_4	1.39	1.38	C_3-C_2-C_{12}	123.51	124.41	C_2-C_1-C_9-C_{10}	-0.05	-0.21
C_3-H_{20}	1.09	1.1	C_2-C_3-C_4	119.36	119.5	H_{11}-C_1-C_9-C_8	0.11	0.03
C_4-C_{10}	1.43	1.44	C_2-C_3-H_{20}	121.28	119.13	H_{11}-C_1-C_9-C_{10}	-179.84	179.45
C_4-H_{21}	1.09	1.1	C_4-C_3-H_{20}	119.36	121.26	C_1-C_2-C_3-C_4	-0.05	1.17
C_5-C_6	1.39	1.39	C_3-C_4-C_{10}	121.48	121.7	C_1-C_2-C_3-H_{20}	-180	-175.23
C_5-C_{10}	1.43	1.44	C_3-C_4-H_{21}	119.51	119.78	O_{12}-C_2-C_3-C_4	-179.25	178.57
C_5-H_{22}	1.09	1.1	C_{10}-C_4-H_{21}	119.01	118.51	O_{12}-C_2-C_3-H_{20}	0.8	2.17
C_6-C_7	1.43	1.43	C_6-C_5-C_{10}	120.73	120.8	C_1-C_2-O_{12}-C_{13}	178.12	-157.43
C_6-H_{23}	1.09	1.1	C_6-C_5-H_{22}	120.35	120.58	C_3-C_2-O_{12}-C_{13}	-2.63	25.05
C_7-C_8	1.39	1.39	C_{10}-C_5-H_{22}	118.92	118.62	C_2-C_3-C_4-C_{10}	0.03	-0.34
C_7-H_{24}	1.09	1.1	C_5-C_6-C_7	120.1	120.27	C_2-C_3-C_4-H_{21}	-179.91	-179.5
C_8-C_9	1.43	1.44	C_5-C_6-C_{23}	120.35	120.34	H_{20}-C_3-C_4-C_{10}	179.98	175.98
C_8-H_{25}	1.09	1.1	C_7-C_6-C_{23}	119.55	119.39	H_{20}-C_3-C_4-H_{21}	0.04	-3.19
C_9-C_{10}	1.44	1.45	C_6-C_7-C_8	120.5	120.53	C_3-C_4-C_{10}-C_5	-179.95	179.83
O_{12}-C_{13}	1.44	1.48	C_6-C_7-H_{24}	119.4	119.29	C_3-C_4-C_{10}-C_9	-0.01	-0.75
O_{13}-H_{14}	1.1	1.11	C_8-C_7-H_{24}	120.11	120.18	H_{21}-C_4-C_{10}-C_5	-0.01	-0.99
C_{13}-H_{15}	1.1	1.11	C_7-C_8-C_9	120.71	120.75	H_{21}-C_4-C_{10}-C_9	179.92	178.43
C_{13}-C_{16}	1.53	1.58	C_7-C_8-H_{25}	120.35	120.62	C_{10}-C_5-C_6-C_7	-0.01	-0.04
C_{16}-O_{17}	1.24	1.26	C_9-C_8-H_{25}	118.93	118.64	C_{10}-C_5-C_6-H_{23}	180	179.98
C_{16}-O_{18}	1.38	1.42	C_1-C_9-C_8	121.97	122.17	H_{22}-C_5-C_6-C_7	179.97	179.96
O_{18}-H_{19}	0.99	1.03	C1-C_9-C_{10}	119.29	119.17	H_{22}-C_5-C_6-H_{23}	-0.03	-0.03
			C_8-C_9-C_{10}	118.74	118.65	C_6-C_5-C_{10}-C_4	179.93	179.52
			C_4-C_{10}-C_5	122.24	122.42	C_6-C_5-C_{10}-C_9	0	0.11
			C_4-C_{10}-C_9	118.54	118.58	H_{22}-C_5-C_{10}-C_4	-0.04	-0.48
			C_5-C_{10}-C_9	119.22	119	H_{22}-C_5-C_{10}-C_9	-179.97	-179.89
			C_2-O_{12}-C_{13}	119.5	113.01	C_5-C_6-C_7-C_8	0.01	-0.03
			O_{12}-C_{13}-H_{14}	112.59	111.69	C_5-C_6-C_7-H_{24}	-180	179.99
			O_{12}-C_{13}-H_{15}	104.84	105.05	H_{23}-C_6-C_7-C_8	-179.99	179.95
			O_{12}-C_{13}-C_{16}	115.49	114.4	H_{23}-C_6-C_7-H_{24}	0	-0.02
			H_{14}-C_{13}-H_{15}	108.39	109.28	C_6-C_7-C_8-C_9	0	0.03
			H_{14}-C_{13}-C_{16}	107.56	108.32	C_6-C_7-C8-H_{25}	-180	180
			H_{15}-C_{13}-C_{16}	107.67	107.92	H_{24}-C_7-C_8-C_9	-180	-180

	C_{13}-C_{16}-O_{17}	123.66	127.09	H_{24}-C_7-C_8-H_{25}	0.01	-0.03
	C_{13}-C_{16}-O_{18}	113.15	110	C_7-C_8-C_9-C_1	-179.96	179.46
	O_{17}-C_{16}-O_{18}	123.14	122.92	C_7-C_8-C_9-C_{10}	0	0.04
	C_{16}-O_{18}-H_{19}	111.13	102.34	H_{25}-C_8-C_9-C_1	0.04	-0.51
				H_{25}-C_8-C_9-C_{10}	179.99	-179.93
				C_1-C_9-C_{10}-C_4	0.02	1.02
				C1-C9-C_{10}-C_5	179.96	-179.54
				C_8-C_9-C_{10}-C_4	-179.93	-179.54
				C_2-O_{12}-C_{13}-H_{14}	53.7	41.76
				C_2-O_{12}-C_{13}-H_{15}	171.32	160.11
				C_2-O_{12}-C_{13}-C_{16}	-70.37	-81.74
				O_{12}-C_{13}-C_{16}-O_{17}	153.92	83.45
				O_{12}-C_{13}-C_{16}-O_{18}	-28.6	-96.71
				H_{14}-C_{13}-C_{16}-O_{17}	27.25	-41.84
				H_{14}-C_{13}-C_{16}-O_{18}	-155.26	138.01
				H_{15}-C_{13}-C_{16}-O_{17}	-89.36	-160.04
				H_{15}-C_{13}-C_{16}-O_{18}	88.12	19.8
				C_{13}-C_{16}-O_{18}-H_{19}	-179.3	179.46
				O_{17}-C_{16}-O_{18}-H_{19}	-1.8	-0.69

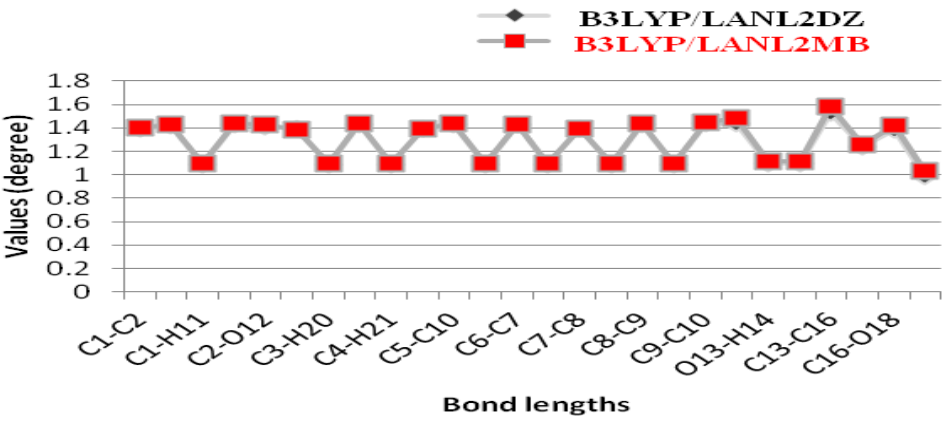

Fig. 3 Bond length of Naphthalene-2-loxy acetic acid

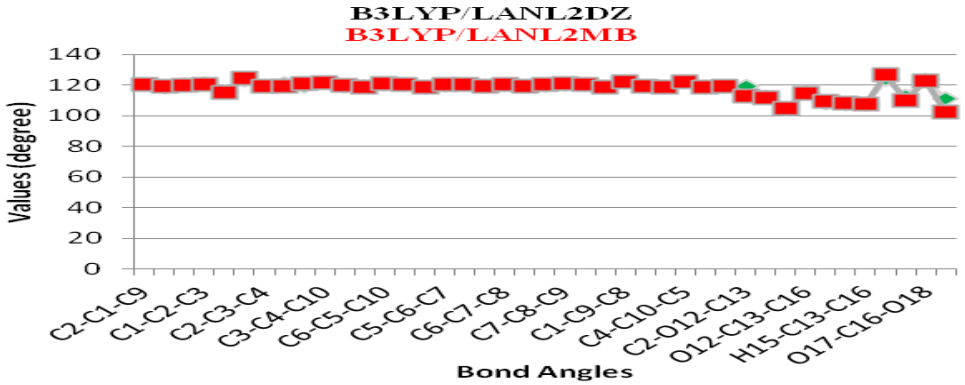

Fig. 4 Bond Angle of Naphthalene-2-loxy acetic acid

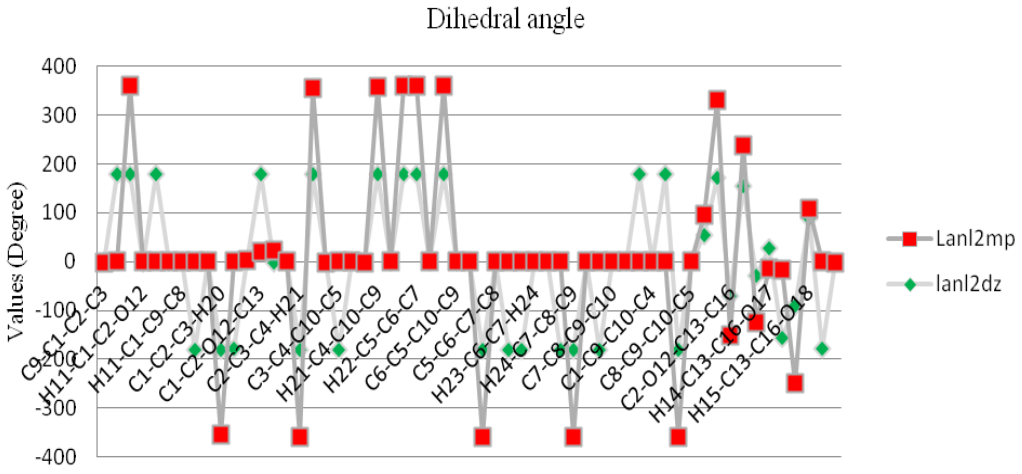

Fig. 5 Dihedral angle of Naphthalene-2-loxy acetic acid

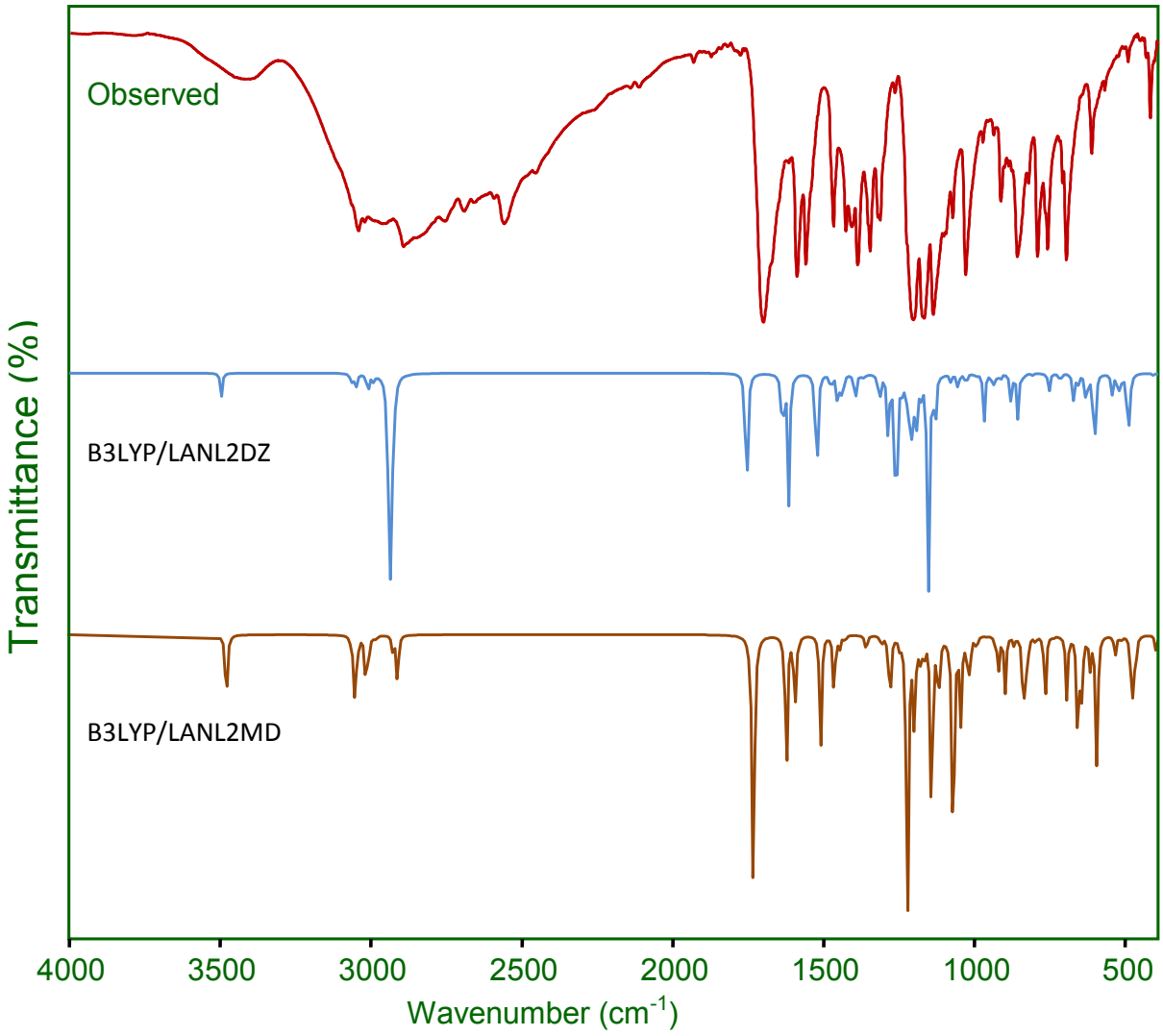

Fig. 6 FT-IR spectrum for Naphthalene-2-yloxy acetic acid

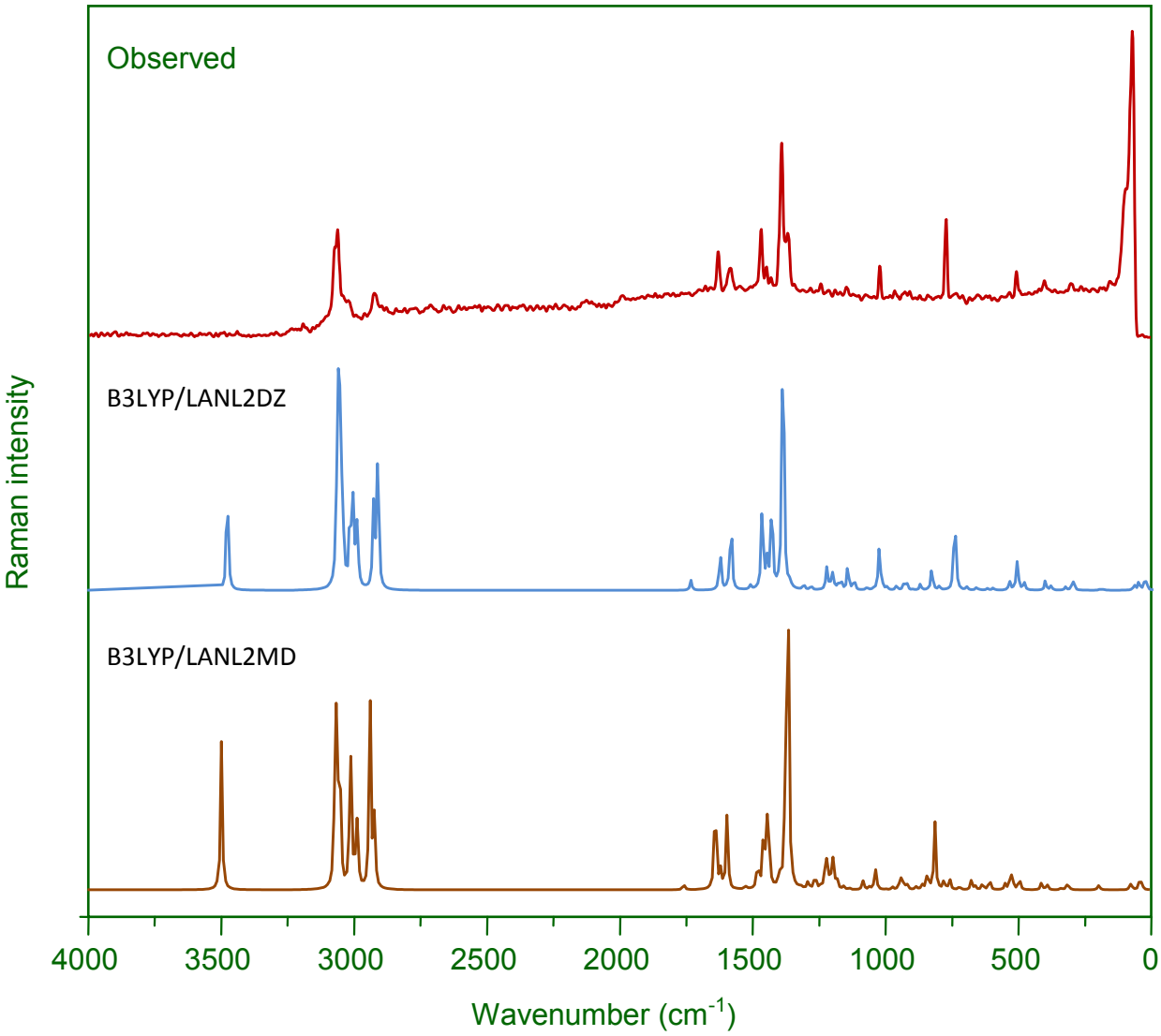

Fig. 7 FT-Raman spectrum for Naphthalene-2-yloxy acetic acid

Table 3

The calculated FT-IR and FT-Raman spectrum of NLA molecule.

Mode No.	Species	Observed Frequency		Calculated Frequency				IR Intensity		Raman activity		VIBRATIONAL ASSINGNMENTS /TED %
		FT-IR	FT RAMAN	B3LYP/LANL2DZ		B3LYP/LANL2MB		B3LYP/ LANL2DZ	B3LYP/ LANL2MB	B3LYP/ LANL2DZ	B3LYP/ LANL2MB	
				Unscaled	scaled	Unscaled	Scaled					
1	A'	3478w	3475 vw	3647	3475	3686	3496	49.88	13.39	126.67	138.51	νOH(100)
2	A'	3060 s		3229	3061	3473	3066	6.34	5.42	227.73	175.86	νCH(39),νCH(33),νCH(14),νCH(12)
3	A'		3051vw	3227	3050	3464	3056	45.46	2.21	195.49	53.29	νCH(32),νCH(26),νCH(20),νCH(20)
4	A'	3040 w		3222	3041	3461	3048	7.43	6.75	45.19	62.98	νCH(94)
5	A'			3209	3014	3453	3016	36.12	3.18	73.85	19.22	νCH(70),νCH(11)
6	A'			3196	3003	3451	3008	7.24	7.31	77.46	101.72	νCH(27),νCH(21),νCH(16)
7	A'			3192	2990	3444	2993	1.00	3.74	60.17	11.19	νCH(25)
8	A'	2981 w		3185	2980	3415	2984	2.18	0.32	10.34	51.80	νCH(65),νCH(35)
9	A'		2924 s	3149	2925	3365	2936	9.56	276.76	82.66	149.00	$\nu ass CH_2$(98)
10	A'	2912w		3085	2910	3290	2920	32.94	4.87	140.10	55.09	$\nu ss CH_2$(65),νCH(35)
11	A'	1738w		1761	1735	1846	1755	225.78	87.39	7.53	3.73	νC=O(80)
12	A'	1628s	1629 s	1687	1626	1760	1636	95.21	40.31	27.74	67.95	νCC(17)
13	A'	1599s		1649	1598	1745	1615	48.74	79.45	1.67	11.06	νCC(29),νCC(17),νCC(13)
14	A'		1584w	1620	1585	1698	1592	4.37	0.60	54.37	42.77	νCC(21),νCC(14),νCC(10),CC(10)
15	A'	1508vs	1513vw	1553	1512	1637	1523	67.75	73.43	2.78	1.98	νCC(12),νHC(17)
16	A'	1468s	1469s	1505	1468	1600	1476	39.37	9.49	61.31	16.09	δHCH(64)
17	A'	1449s	1448ms	1500	1450	1595	1453	7.88	22.49	18.81	38.26	scissHCC(11),scissHCC(10)
18	A'	1430s		1475	1432	1556	1437	3.30	16.60	67.20	60.15	δCH(17),δCH(13)
19	A'	1389m	1391s	1444	1390	1488	1395	0.08	19.55	204.48	8.06	νCC(32)
20	A'		1367ms	1416	1365	1473	1371	5.32	2.69	2.86	67.54	νCC(17),νCC(14)
21	A'	1357ms		1398	1360	1454	1362	4.89	0.78	0.89	169.64	δCH(34),δCH(10)
22	A'	1308w	1313vw	1394	1312	1445	1315	6.10	17.99	3.61	1.16	$rock CH_2$(15)
23	A'			1362	1284	1422	1286	48.24	41.23	2.61	4.42	δOH(29),δOH(26),δOH(13)
24	A'	1249w	1250s	1308	1251	1358	1260	7.44	112.71	0.09	8.52	δHC(18),δCH(17),δCH(11)
25	A'		1225ms	1301	1226	1341	1237	177.36	11.18	14.97	1.98	δHCC(16),δCC(15),δHCC(10)

26	A'	1213w		1284	1214	1331	1219	6.02	31.53	3.58	23.88	δHCO(44),βHCOC(13)
27	A'		1200w	1254	1203	1303	1206	54.57	37.56	10.69	4.23	νCC(14),νCC(13)
28	A'	1183s		1203	1185	1267	1194	15.34	32.91	3.58	19.85	δHCC(23)
29	A'		1175w	1202	1172	1253	1179	14.74	15.27	6.57	7.29	δHCC(28),δHCC(14)
30	A'	1149vs	1147w	1196	1146	1228	1153	121.45	131.17	16.34	1.67	δCH(25),δHCO(10)
31	A'	1119s	1125w	1158	1123	1222	1131	43.34	35.27	6.62	0.91	δHCC(18),δHCC(13)
32	A'	1077s		1123	1075	1208	1079	167.61	4.64	1.78	4.83	δOH(14),δOH(13)
33	A'		1051w	1061	1050	1100	1054	51.80	9.07	0.64	1.73	νCO(59)
34	A'			1041	1030	1089	1033	12.26	0.15	25.28	9.87	νCH(48),νHCC(10)
35	A'	1021w	1022ms	1038	1020	1065	1028	24.93	6.61	6.46	1.90	δCCH(54),δCCC(31)
36	A'		1000w	1035	1001	1050	1004	0.01	0.00	1.40	0.07	γHCCH(65),γHCCC(12),γHCCC(10)
37	A'	985w	988w	1014	988	1025	995	7.33	1.55	0.27	0.33	γHCCH(70),γHCCC(16)
38	A'	963w	963w	994	964	1015	968	0.49	27.34	2.76	1.27	νCCCH(14),νCH(14)
39	A'	936w		966	935	992	939	6.12	7.69	5.04	6.90	δCCC(20),δCCC(20)
40	A'		925w	943	925	930	931	21.51	2.79	3.46	3.84	γCCCH(51)
41	A'	909ms	900w	899	903	925	915	35.23	4.38	0.41	3.81	τ CCCH(51)
42	A'	872ms	875w	895	874	912	879	5.64	16.21	3.55	1.43	τ CCCH(33), τ HCCC(23), τ HCCC(18)
43	A'	843s		847	843	893	856	55.15	26.00	0.66	2.18	τ CCCH(44), τ CCCH(24), τ HCCC(10)
44	A'		830w	836	831	857	837	21.75	2.36	13.65	9.42	νCCO(50),νCCO(17),νOCC(15)
45	A'	806vs	800w	806	803	809	809	3.77	0.96	2.48	35.14	νassCCC(22),νCC(19),νCC(10)
46	A'	764w	770vs	787	771	803	774	38.19	0.34	0.01	4.50	τ CCCH(57), τ CCCH(14), τ CCCH(11)
47	A'	748s		777	745	793	753	1.08	10.77	48.04	4.86	νCC(44), νCC(14), νCC(12)
48	A'		713ms	705	712	722	716	39.10	4.99	1.69	1.71	νOC(15)
49	A'	666s		676	663	695	671	67.57	16.05	1.55	4.54	γOH(37),γOH(12)
50	A'		650w	667	650	674	656	36.53	5.32	0.21	1.52	Ring-γ(64)
51	A'	623w	625s	639	623	651	629	19.02	19.63	0.91	3.39	γHOCC(37),νassCCC(16),νassCCC(12)
52	A'		600w	614	601	638	603	84.68	53.53	1.22	5.21	γHCOC(51)
53	A'	547s	539ms	556	540	566	544	12.24	11.75	4.67	2.63	Ring-γ CCCC (20)
54	A'	508vw	508vs	548	521	542	523	3.17	13.23	1.37	9.97	γCH(26),γCH(10)
55	A'	487ms		524	510	529	512	0.22	2.50	16.08	1.47	Ring breathingCCCC(17),CCCC(12)
56	A'	474vs	475w	519	485	506	491	44.67	45.46	4.82	5.61	γCOOH(57), τ CCCC(10)
57	A'			496	473	491	479	23.56	4.03	0.03	0.06	Rin-(34),τCCCC(24),τCCCC(14)

58	A'		460	405	420	407	10.01	1.04	5.12	3.02	$\omega CH_2(39)$, $\omega CH_2(15)$
59	A'		419	384	407	386	0.23	1.12	2.23	2.62	γCCCH(17),γCCCH(12),τCCCH(12)
60	A'		387	330	388	333	0.95	3.35	1.80	0.88	Ring-δ (22), γCCC(16)
61	A'	302ms	322	304	323	309	2.02	1.52	3.82	3.21	ν_{sym}CCO(28)
62	A'	298w	317	298	311	300	2.91	1.56	2.84	0.37	ν_{sym}CCO(32)
63	A'		236	200	208	201	1.81	2.25	0.57	0.10	twistCCO(10)
64	A'	188w	199	190	204	192	2.75	0.18	0.34	1.74	ωCOC(18),ωCCO(10)
65	A'		189	182	189	181	0.74	1.10	0.14	0.22	τCCCC(19)
66	A'	71vs	113	72	125	73	0.31	2.29	2.64	0.78	γCOC(26),τCCCC(11)
67	A'		57	64	87	69	0.31	2.60	4.53	2.52	τCCCO(24),τCOCC(19),τOCCO(16)
68	A'		30	37	67	39	0.18	0.08	5.44	2.82	τCOOH(26),τCOOH(17)
69	A'		25	30	29	30	1.70	0.73	2.24	3.11	τCOOH(41)

s-strong, ms-medium strong, w-weak, vw-very weak, vs-very strong, ν-stretching, ν_{sym}-sym stretching, ν_{asym}-asym stretching, δ-in-plane bending, γ-out-of-plane bending, scis-scissoring, ω-wagging, rock-rocking, τ-torsion(out-of-plane bending)..

8. O-H vibrations

The hydroxyl stretching vibrations are generally [10] observed in the region around 3500 cm^{-1}. The peak is broader associated its intensity is on the far side that of a free OH vibration that indicates involvement in associate to the intermolecular hydrogen bond. Hydroxyl group of compounds containing active hydrogen grouping endure self-association and their spectra are consequently terribly hooked on the state of the sample. Hydroxyl radical compounds in solid and pure liquid state ordinarily exist as compound aggregates command along by hydrogen bonds that break upon dilution, to monomers. The extremely hindered hydroxyl group displays a free O-H stretching wavenumber even within the pure state for NLA exhibits a free O-H stretching. Hydrogen bonding alters the wavenumbers of the stretching and bending vibrations. The O-H stretching bands move to lower wavenumbers usually with accumulated intensity and band broadening within the hydrogen-bonded species. In the present study, the stretching vibrations of the hydroxyl group of NLA was observed in IR at 3478 cm^{-1} and in Raman observed at 3475 cm^{-1}. The O-H in-plane bending vibration is generally observed within the region from 1650 to1589 cm^{-1}, the position of the band depending on the type of the hydroxyl group [11].

As seen from the PED values shown in Table.3, the O-H in-plane vibrations are powerfully mixed with other vibrations. The O-H vibration is incredibly a harmonic so it is difficult to reproduce this wavenumber with a harmonic approach. For NLA, the wavenumber of this in-plane bending vibration was observed at IR in 1200 and 1077 cm^{-1} and out-of-plane bending vibration was observed in Raman at 666 and 487 cm^{-1}.

9. C-H Vibrations

The aromatic structure shows the presence of C-H stretching vibrations around 3000 cm^{-1}. In the present work, the C-H stretching vibration of the naphthalene ring is ascertained within the FT-IR spectrum at 3060, 3040, 2981 and 2912 cm^{-1} and within the FT-Raman spectrum at 3051 and 2924 cm^{-1}. The vibration is calculated in the range 3061-2984 cm^{-1} by the B3LYP/LANL2MB method and this shows sensible correlation with the experimental data. The C-H in-plane bending vibrations are observed in the region 1100-1400 cm^{-1} and are typically weak. These vibrations are observed in the FT-IR spectrum at 1468, 1430, 1357, 1249, 1213, 1183, 1149, 1119 and 1021 cm^{-1} and Raman spectrum at 1469, 1313, 1250, 1147, 1125 and 1022 cm^{-1}. The C-H out-of-plane bending modes arise in the region 600-900 cm^{-1} [12- 14]. These modes observed in the FT-IR spectrum at 985, 963, 843, 806 and 764 cm^{-1} and Raman spectrum at 1000, 988, 963, 800 and 770 cm^{-1}. The C-H out-of-plane bending modes for NLA are also assigned to the characteristic region and are given in Table.3.

10. C-C Vibrations

The bands that indicate aromatic properties of benzene derivatives principally occur among the range of 1625-1200 cm^{-1}. The particular positions of those modes are determined not such a lot by the nature of the substituents by the form of substitution around the ring, though significant halogens undoubtedly diminish the frequency [15, 16]. The medium to very strong lines observed within the IR spectrum of NLA at 1628, 1599, 1508, 1389 and 748 cm^{-1} and in Raman spectrum to the strong lines observed at 1629, 1584, 1513, 1391, 1367 and 1200 cm^{-1} are ascribed to the C-C stretching modes. The modes observed at 936 are assigned to the C-C in-plane bending vibrations of NLA. The CC out-of-plane bending modes of NLA is attributed to the Raman frequency is ascertained at 650 cm^{-1}. The theoretical

CC out-of-plane bending modes are given in Table 3. The CC stretching, in-plane and out-of-plane bending vibrations are represented as mixed as there are about 15-30% of PED contributions.

11. C=O and C-O vibrations

The C=O stretch of carboxylic acids is identical to the C=O stretch in ketones, that is expected in the region 1740-1660 cm^{-1}[17-19]. In the present study, a very strong band was observed within the FT-IR spectrum at 1738 cm^{-1} is assignable C=O stretching vibrations deviate from the B3LYP/LANL2DZ predicted value 1735 cm^{-1} shows by 3 cm^{-1}. The FT-Raman data and the PED value of 80% are reported in Table 3. The C-O stretching vibration are assigned to 1051, 830, 713 and 302 cm^{-1} (60-15%).

12. HOMO-LUMO Analysis

HOMO, LUMO and frontier orbital gap being important parameters for quantum chemistry helps to exemplify the chemical reactivity and kinetic stability of the molecules [20]. The HOMO is the orbital that primarily acts as an electron donor and therefore the LUMO is that the orbital that primarily acts as an electron acceptor. HOMO and LUMO energies and orbital energy gap were computed at B3LYP/LANL2DZ in NLA. The results belong to those calculations were presented in Table 4. The 3D drawing of the frontier orbitals of NLA is pictured in Fig. 8. It may be seen from the plot of HOMO level, all positive and negative regions are unfold entire the molecule. In LUMO level, positive and negative regions that are distributed as symmetric are spread entire the molecule. The energy gap between HOMO-LUMO explains the ultimate charge transfer interaction among the molecule. The frontier orbital energy gap just in case of NLA is found to be 3.66347065 eV. The narrow energy gap between HOMO and LUMO facilitates intramolecular charge transfer which makes the material to be NLO active [21].

The electronegativity (χ), chemical hardness (η) and chemical potential (μ) be necessary tools to check the order of stability of molecular systems have given in Table.4. The chemical hardness (η) and chemical potential (μ) are calculated using HOMO and LUMO energies. Electronegativity (χ) is defined as negative of the chemical potential. The chemical hardness may be a smart indicator of the chemical stability. The molecules having a tiny low energy gap are known as soft and having a large energy gap is understood as hard molecules [22, 23]. The chemical hardness value is 0.13831 eV for gases phase.

In frontier region, neighboring orbitals may show similar degenerate energy levels. In such cases thought of only HOMO and LUMO may not yield a sensible description of frontier orbitals. In this reason, density of states (DOS), overlap population density of states (OPDOS) or crystal orbital overlap population (COOP) are the total of alpha (α) and beta (β) electron density of states [24, 25], in terms of Mulliken population analysis are calculated and plotted in Fig. 9a and 9b they provide a pictorial representation of molecule orbital compositions and their contributions to their chemical bonding. The Density Of State plots are to demonstrate the composition of FOs contributing to the molecular orbitals. OPDOS can enable us to determine bonding, non-bonding and anti-bonding characteristics with relevancy specific fragments. A positive value in OPDOS plots suggests that a bonding interaction, whereas a negative value represents an anti-bonding interaction and a value close to zero indicates a nonbonding interaction. PDOS mainly presents the composition of fragment orbitals contributing to molecular orbitals. αβDOS shows the bonding, sum of positive and negative electron with nature of interaction of two orbitals, atoms or groups. In NLA there exists 53α and β-electrons, totally 106 electrons are occupied in DOS. This way designates that a image representation for cations and anions is necessary similar to that for neutral atoms in their ground state. Positive value of αβDOS indicates a bonding interaction,

negative value indicates an anti-bonding interaction and zero value indicates nonbonding interactions [27].

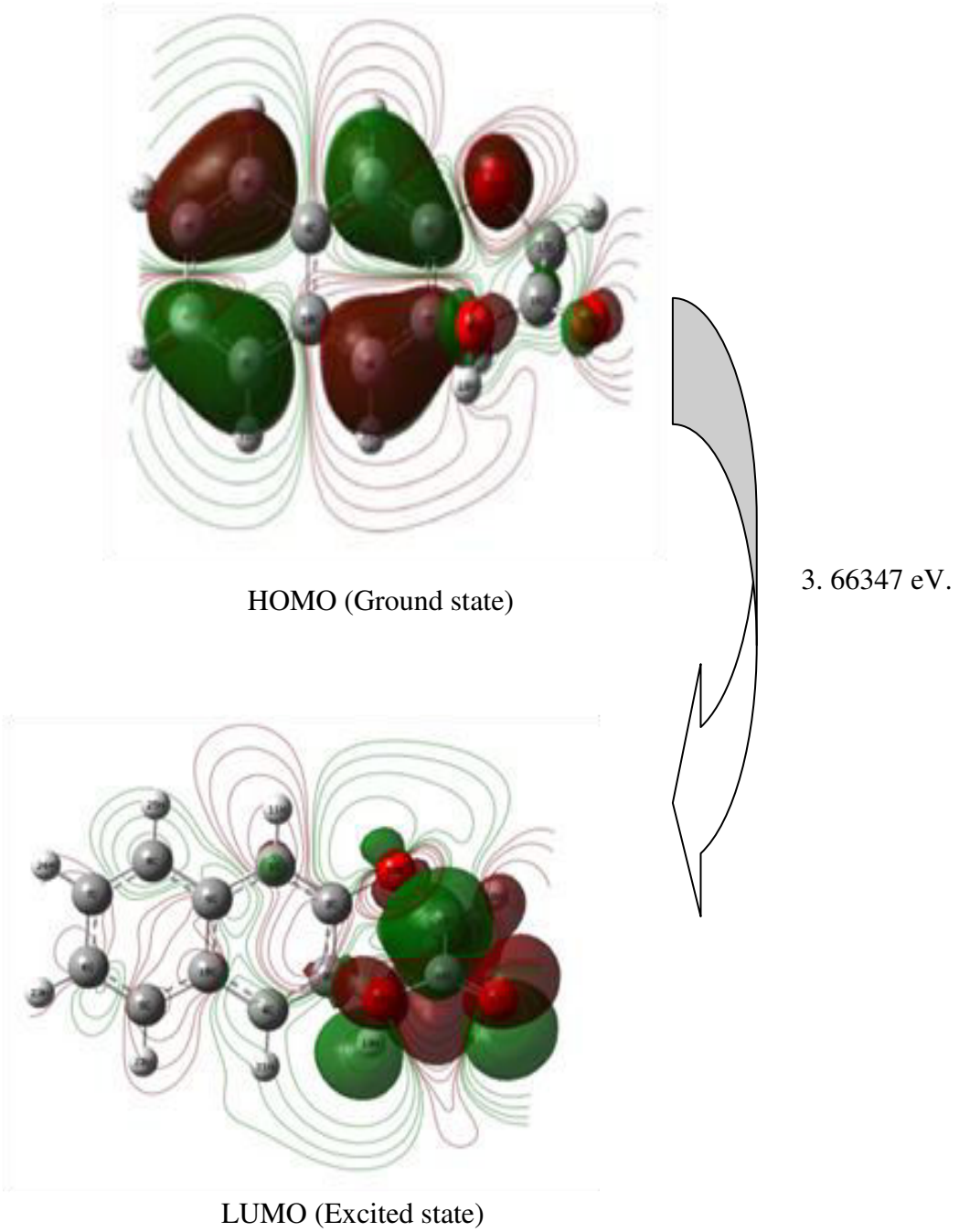

Fig. 8 The atomic orbital composition of the frontier molecular orbital for title compound

Table 4

HOMO and LUMO energies gap values (ev) and related molecular properties of Naphthalen - 2 - lyoxy acetic acid based on B3LYP/LANL2DZ method.

Molecular properties	E_{HOMO}	E_{LUMO}	E_{HOMO-1}	E_{LUMO+1}	E_{HOMO-2}	E_{LUMO+2}
Energy (eV)	-5.9685483	-2.3050776	-6.1897769	-1.1137626	-7.7879024	-0.2604131
Energy gap (eV)	3.66347065		5.07601437		7.52748932	
Ionization potential (I)	0.21934		0.22747		0.2862	
Electron affinity (A)	0.08471		0.04093		0.00957	
Global hardness (η)	0.06731		0.09327		0.13831	
Electro negativity (χ)	0.05332		0.1342		0.14788	
Chemical softness (π)	14.85552		10.72156		7.23013	
Chemical potential (μ)	-0.05332		-0.1342		-0.14788	
Global Electrophilicity (ω)	0.21117		0.0651		0.07902	

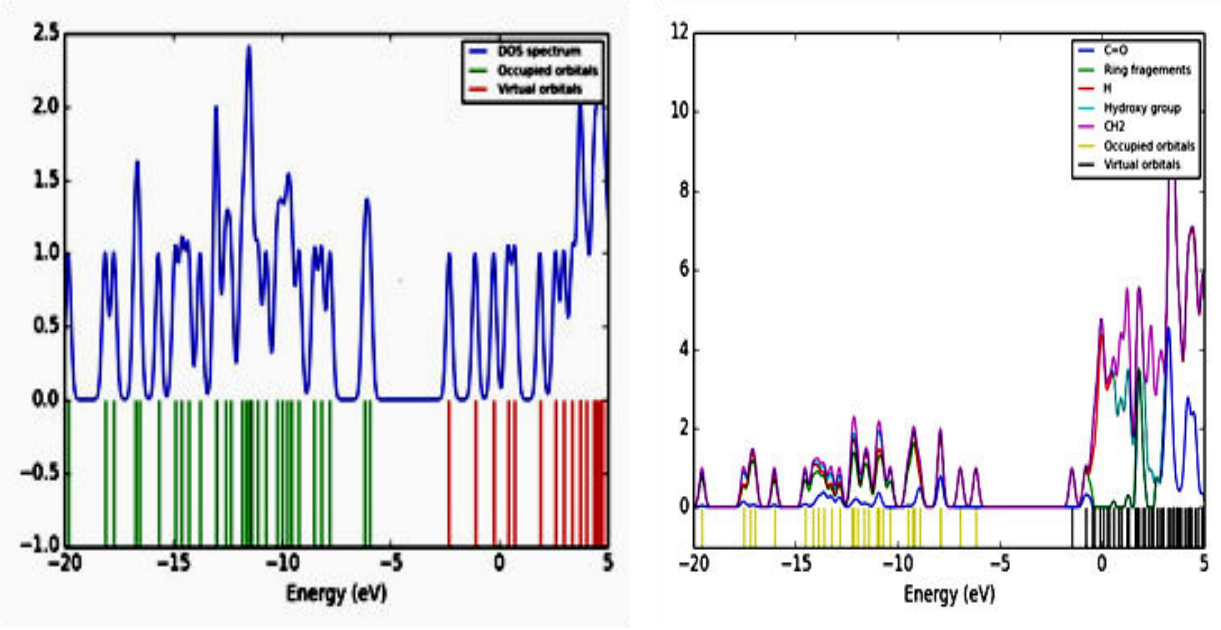

Fig. 9 a,b DOS and OPDOS diagram for Naphthalene-2-yloxy acetic acid

13. Mulliken atomic charge analysis

It is clear that Mulliken populations are yield one of the every of best footage of charge distribution and Mulliken charges render net atomic populations among the molecule. The charge distributions of NLA have been calculated by B3LYP/LANL2DZ level of theory. The results are given in Table 5. As are often seen from the Table 5, the magnitudes of the carbon atomic charges, found to be either positive or negative, were noted to alter from -0.566454 to 0.398937 eV. All the hydrogen atoms have a positive charge and every one oxygen atoms have a negative charge. The Carbon (C_2) atom has the most positive charge than the other carbon atoms; thus it is an acceptor atom. It is also observed that C_7 and every one

oxygen atoms have maximum negative charge (C_7, O_{12}, O_{17} and O_{18}) and thus they act as donor atoms. The graphical represent of Mulliken atomic charges are shown in Fig.10.

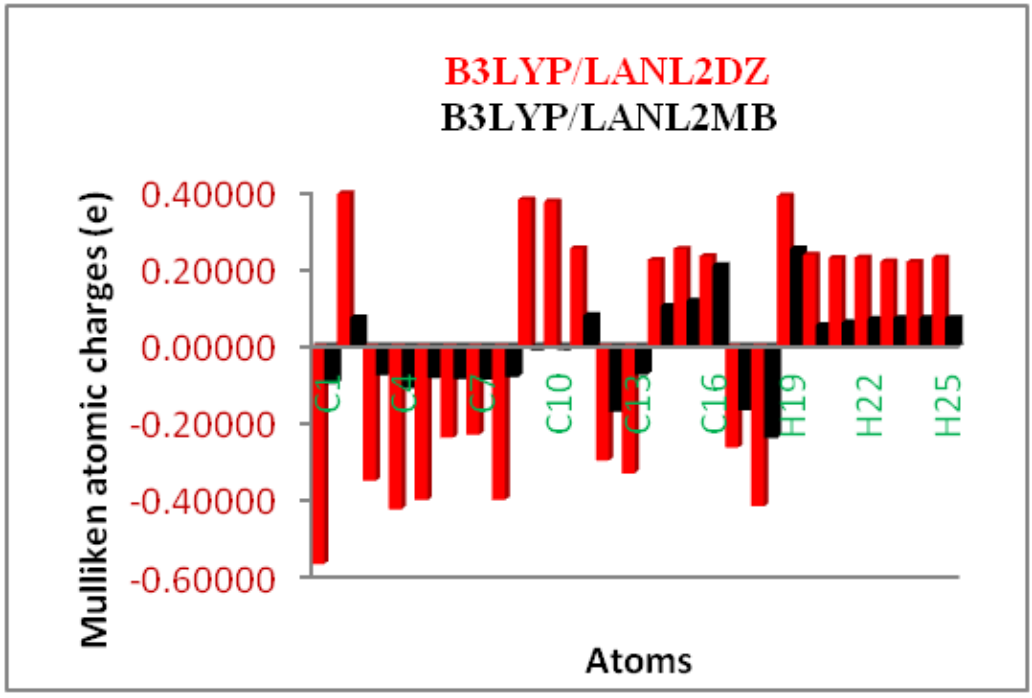

Fig. 10 Comparative Milliken's plot by B3LYP/LANL2DZ and LANL2MB level for C8 conformer of Naphthalene-2-yloxy acetic acid.

14. Nonlinear optical (NLO) effects

In the recent times, a large number research of new materials exhibiting efficient NLO options has been of great interest as a result if potential applications as fashinable communication technology, telecommunication, and optical signal processing [28-31]. It is familiar that the importance of the polarizability and thus the first hyperpolarizability of molecular systems is

Table 5

Mulliken's population analysis of Naphthalene-2-yloxy Acetic Acid at B3LYP/LANL2DZ and B3LYP/LANL2MB methods

Atom No.	Mulliken atomic charges		Atom No.		
	B3LYP/ LANL2DZ	B3LYP/ LAN2MB		B3LYP/ LANL2DZ	B3LYP/ LAN2MB
C_1	-0.566454	-0.096266	C_{13}	-0.329960	-0.072565
C_2	0.398937	0.075940	H_{14}	0.226056	0.106397
C_3	-0.348688	-0.073951	H_{15}	0.254513	0.120046
C_4	-0.423164	-0.107178	C_{16}	0.235786	0.212292
C_5	-0.398821	-0.081587	O_{17}	-0.262596	-0.164773

C_6	-0.236453	-0.084092	O_{18}	-0.415438	-0.238044
C_7	-0.228761	-0.084855	H_{19}	0.393508	0.255872
C_8	-0.398802	-0.079161	H_{20}	0.239321	0.056477
C_9	0.383797	-0.009085	H_{21}	0.231011	0.063179
C_{10}	0.378647	-0.008424	H_{22}	0.232152	0.072100
H_{11}	0.255670	0.081654	H_{23}	0.221614	0.074687
O_{12}	-0.295808	-0.168371	H_{24}	0.221253	0.075000
			H_{25}	0.232678	0.074708

depends on the potency of transmission between acceptor and also the donor groups as which will be the key to intra molecular charge transfer [32-33]. The acceptor and donor groups have an crucial role witin the polarizability and first hyperpolarizability. The higher value of first hyperpolarizability measured of the NLO activity of the molecular system is related to the ensuing from the electron cloud movement through π conjugated frame work from electron donor to electron acceptor groups [34].

The calculated NLO properties by the B3LYP/LANL2DZ as the components of the dipole moments μ (Debye), static polarizability components α (a.u.), the typical polarizability (or linear polarizability) α_o ($\times 10^{-24}$ esu), the anisotropy of the polarizability, $\Delta\alpha(A^o)$, and therefore the first hyperpolarizability components $\beta_\circ$($\times 10^{-33}$ esu) of Naphthalene-2-yloxy acetic acid and tabulated in Table 6. The μ_o, α_o, $\Delta\alpha$, β, $\beta_\circ$ of the title molecule are often calculated by using the subsequent equations, respectively.

$$\mu_\circ = (\mu_x^2 + \mu_y^2 + \mu_z^2)^{1/2}$$

$$\alpha_\circ = \frac{(\alpha_{xx}+\alpha_{yy}+\alpha_{zz})}{3}$$

$$\Delta\alpha = \frac{1}{\sqrt{2}}[(\alpha_{xx} - \alpha_{yy})^2+(\alpha_{yy} - \alpha_{zz})^2+(\alpha_{zz} - \alpha_{yy})^2+6\alpha_{xx}^2]^{1/2}$$

$$\beta_x = (\beta_{xxx} + \beta_{xyy} + \beta_{xzz})$$

$$\beta_y = (\beta_{yyy} + \beta_{xxy} + \beta_{yzz})$$

$$\beta_z = (\beta_{zzz} + \beta_{xxz} + \beta_{yyz})$$

$$\beta_\circ = (\beta_x^2 + \beta_y^2 + \beta_z^2)^{1/2}$$

Table 6

Electric dipole moment μ(debye), mean polarizabilityα_{tot}(e.s.u.), anisotropy polarizability $\Delta\alpha$(e.s.u.) and first order hyperpolarizability β_{tot} ($\times 10^{-30}$ e.s.u.) for Naphthalene-2-yloxy Acetic Acid at B3LYP/LANL2DZ and B3LYP/LANL2MB methods.

Parameters	B3LYP		Parameters		
	LANL2DZ	LANL2MB		LANL2DZ	LANL2MB
μ_x	0.5040	-0.2221	$\Delta\alpha$	2.5089×10^{-30}	1.15157×10^{-30}
μ_y	-0.4658	-0.8559	β_{xxx}	374.0593	489.1451
μ_z	0.8661	0.2935	β_{yyy}	126.0521	277.3080
μ	1.1050	0.9317	β_{zzz}	54.5758	173.1071

α_{xx}	196.7948	148.2150	β_{xyy}	-31.6672	86.1443
α_{xy}	44.2916	37.7562	β_{xxy}	91.9878	126.2246
α_{xz}	152.8049	107.5787	β_{xxz}	41.3716	96.7738
α_{yy}	7.7923	7.5769	β_{xzz}	1.2884	63.0421
α_{yz}	10.0041	8.8185	β_{yzz}	40.9002	61.8547
α_{zz}	66.3263	26.2033	β_{yyz}	3.0494	40.2406
α	5.2408	7.8014	β_{xyz}	42.3955	31.3768
			β_{tot}	3.8145×10^{-30}	7.3315×10^{-30}

The calculated $\mu_{o,}$ $\alpha_{o,}$ $\Delta\alpha$, $\beta_{\circ}$ values of NLA of 1.1050 Debye, 5.2408 e.s.u, 2.5089×10^{-30} e.s.u 3.8145 $\times10^{-30}$ esu, respectively. Urea is one of the archetypical molecules utilized in the study of the NLO properties of molecular systems. Thus it had been used frequently as a threshold value for comparative functions. The calculated value of $\beta_{\circ}$ for the title compound is comparatively higher than that of urea. Thus NLA molecule may be a good candidate of NLO material.

15. Natural bond orbital (NBO) analysis

NBO analysis provides a possible "Natural Lewis structure", as result of all orbital details are mathematically chosen to include the perfect potential share of the electron density. A useful aspect of the NBO method is that it provides info concerning intra and intermolecular bonding and interactions among the bonds, and also provides a convenient basis for investigation the interactions in each stuffed and virtual orbital areas along with charge transfer and conjugative interactions in molecular system. The second order Fock matrix was administered to guage donor-acceptor interactions within the NBO analysis [35]. The interaction result in a loss of occupancy from the localized NBO of the perfect Lewis structure into an empty non-Lewis orbital. For every donor (i) and acceptor (j), the stabilization energy E_2 related to the delocalization i→ j is estimated as

$$E_2 = \Delta_{ij} = q_i \frac{F(i,j)^2}{\varepsilon_j - \varepsilon_i}$$

wherever q_i is that the orbital occupancy, ε_i and ε_j are diagonal elements and F(i,j) is that the off diagonal NBO Fock matrix element. Some electron donor orbital, acceptor orbital and therefore the interacting stabilization energy resulted from the second-order-microdesturbance theory are reported [36]. The larger the E(2) value, the heap intensive is that the interaction between electron donors and electron acceptors, i.e., that a lot ofdonating tendency from electron donors to electron acceptors and so the larger extent of conjugation of the complete system. Delocalization of electron density between occupied Lewis sort (bond or lone pair) NBO orbitals and formally unoccupied (antibonding and Rydgberg) non-Lewis NBO orbitals correspond to a stabilization donor-acceptor interaction. NBO analysis has been performed on the molecule using NBO 3.1 program was implemented among the Gaussian 09W package at the DFT-B3LYP/LNA2DZ level of theory so as to elucidate the intramolecular interaction, rehybridization and delocalization of electron density inside the molecule. The corresponding results are tabulated in Table 7. The natural bonding orbital analysis aditionally describes the bonding in terms of the natural hybrid orbital of σ(O18-H19), that occupy a higher energy orbital (-0.79201 a.u) with appreciable p-character (78.89%) and occupation number (1.96572 a.u). The other orbital interactions are given in Table 8.

The intramolecular hyperconjugative interactions are formed by the orbital overlap between bonding (C-C), (C-O), (O-H) and antibonding (C-C), (C-O), (C-H) orbital which ends up in intramolecular charge transfer (ICT) causing stabilization of the molecular system. These interactions are determined as a rise in electron density (ED) in C-C and C-O antibonding orbital that weakens the individual bonds. The strong intramolecular hyperconjucative interactions of σ and π electrons of C-C, C-O bonds to the anti C-C, C-H bonds of the ring lead to stabilization of some part of the rings as evident form Table 8. There happens a strong intramolecular hyperconjucative interaction of LP electrons from LPC9 to π^*(C1-C2) (ED = 1.01560 e and E(2) = 276.813 kJ mol^{-1}), from π(C1-C2) to π^*(C3-C4) (ED = 1.75081 e and E(2) = 86.3996 kJ mol^{-1}). These interactions give rise to increasing the ED on π^* bonds leading to stabilization of NLA with totally different stabilization energies. This intramolecular charge transfer can induce large nonlinearity to the molecule.

Table 7

Second order perturbation theory analysis of Fock matrix in NBO basis corresponding to intra molecular bands of Naphthalene-2-yloxy Acetic Acid at B3LYP/LANL2DZ and B3LYP/LANL2MB methods.

S.No.	Donor NBO(i)	ED (i) e	Acceptor NBO(j)	ED (j) e	E(2) kJ/mol^{-1}	E(j)-E(i) a.u	F(i,j) a.u
1	$\sigma(C_1-C_2)$	1.97384	$\sigma^*(C_2-C_3)$	0.02000	16.025	1.22	0.061
2	$\pi(C_1-C_2)$	1.75081	$\pi^*(C_3-C_4)$	0.29194	86.3996	0.3	0.071
3	$\sigma(C_1-C_9)$	1.96656	$\sigma^*(C_2-O_{12})$	0.02019	24.309	0.91	0.065
4	$\pi(C_3-C_4)$	1.76137	$\pi^*(C_1-C_2)$	0.29070	68.5339	0.31	0.064
5	$\sigma(C_1-H_{11})$	1.97175	$\sigma^*(C_2-C_3)$	0.01552	26.945	1	0.072
6	$\sigma(C_2-C_3)$	1.97437	$\sigma^*(C_1-C_2)$	0.03554	16.485	1.31	0.064
7	π(C5-C6)	1.74570	$\pi^*(C_7-C_8)$	0.25842	77.5295	0.3	0.067
8	$\pi(C_{16}-O_{17})$	1.98458	$\pi^*(C_{13}-C_{14})$	0.11899	9.0793	0.86	0.039
9	$\pi(C_7-C_8)$	1.74504	$\pi^*(C_5-C_6)$	0.25641	78.9521	0.3	0.067
10	LPC_9	1.01560	$\pi^*(C_1-C_2)$	-	276.813	0.13	0.103
11	LPC_{10}	1.00493	$\pi^*(C_3-C_4)$	-	269.994	0.13	0.1
12	LPO_{12}	1.96645	$\sigma^*(C_2-C_3)$	-	23.514	1.09	0.07
13	LPO_{12}	1.87791	$\pi^*(C_1-C_2)$	-	85.2699	0.37	0.08
14	LPO_{17}	1.97698	$\sigma^*(C_{13}-C_{16})$	-	11.38	1.01	0.047
15	LPO_{17}	1.87395	$\sigma^*(C_{16}-O_{18})$	-	134.683	0.49	0.113
16	LPO_{18}	1.93015	$\pi^*(C_{16}-O_{17})$	-	38.367	0.53	0.063
17	LPO_{18}	1.90050	$\pi^*(C_3-C_4)$	-	89.538	0.45	0.092

F(i, j) is the Fock matrix elements between i and j NBO orbital's.
E(2) – mean energy of hyper conjugative interactions.
E(j) – E(i) – energy difference between donor and acceptor i and j NBO orbital's.

Table 8

NBO results showing the formation of Lewis and non-Lewis orbitals of NLA.

Bond orbital	Occupancies (e)	EDA %	EDB %	Polarization coefficient of bond orbital		Hybrid	S (%)	P (%)
				I Atom	II atom			
C_1-C_2	1.97384 -0.72486	49.65	50.35	0.7046	0.7096	$SP^{1.76}$	36.21	63.79

	1.96656							
C_1-C_9	-0.67354	49.6	50.4	0.7042	0.71	$SP^{1.79}$	35.81	64.19
	1.97175							
C_1-H_{11}	-0.50791	61.68	38.32	0.7854	0.619	$SP^{2.57}$	27.99	72.01
	1.97437							
C_2-C_3	-0.72107	48.84	51.16	0.6989	0.7153	$SP^{1.72}$	36.78	63.22
	1.9848							
C_2-O_{12}	-0.84534	31.51	68.49	0.5613	0.8276	$SP^{3.25}$	23.54	76.46
	1.97358							
C_3-C_4	-0.73236	51.34	48.66	0.7165	0.6976	$SP^{1.63}$	38.02	61.98
	1.96713							
C_3-H_{20}	-0.56448	59.33	40.67	0.7703	0.6377	$SP^{2.62}$	27.63	72.37
	1.96971							
C_4-C_{10}	-0.67229	49.55	50.45	0.7039	0.7103	$SP^{1.81}$	35.6	64.4
	1.97447							
C_4-H_{21}	-0.51670	60.8	39.2	0.7798	0.6261	$SP^{2.60}$	27.8	72.2
	1.97965							
C_5-C_6	-0.70480	50.27	49.73	0.709	0.7052	$SP^{1.74}$	36.54	63.46
	1.97109							
C_5-C_{10}	-0.67130	48.86	51.14	0.699	0.7152	$SP^{1.83}$	35.29	64.71
	1.97622							
C_5-H_{22}	-0.50704	60.83	39.17	0.7799	0.6259	$SP^{2.55}$	28.13	71.87
	1.97798							
C_6-C_7	-0.67449	50.02	49.98	0.7072	0.707	$SP^{1.86}$	34.92	65.08
	1.97598							
C_6-H_{23}	-0.50501	61.1	38.9	0.7817	0.6237	$SP^{2.54}$	28.23	71.77
	1.97951							
C_7-C_8	-0.70456	49.74	50.26	0.7052	0.709	$SP^{1.72}$	36.82	63.18
	1.97585							
C_7-H_{24}	-0.50432	61.12	38.88	0.7818	0.6235	$SP^{2.54}$	28.25	71.75
	1.97054							
C_8-C_9	-0.06712	48.83	51.17	0.6988	0.7153	$SP^{1.84}$	35.24	64.76
	1.97603							
C_8-H_{25}	-0.50562	60.97	39.03	0.7809	0.6247	$SP^{2.55}$	28.15	71.85
	1.96274							
C_9-C_{10}	-0.67342	49.98	50.02	0.707	0.7072	$SP^{1.98}$	33.59	66.41
	1.98454							
O_{12}-C_{13}	-0.82942	66.9	33.1	0.8179	0.5753	$SP^{3.04}$	24.75	75.25
	1.96903							
C_{13}-H_{14}	-0.57919	61.02	38.98	0.7811	0.6244	$SP^{2.86}$	25.91	74.09
	1.97052							
C_{13}-H_{15}	-0.57033	62.55	37.45	0.7909	0.6119	$SP^{2.64}$	27.49	72.51
	1.98547							
C_{13}-H_{16}	-0.69982	49.71	50.29	0.705	0.7092	$SP^{2.88}$	25.79	74.21
	1.99514							
C_{16}-O_{17}	-1.07206	33.19	66.81	0.5761	0.8174	$SP^{2.07}$	32.59	67.41
	1.99086							
C_{16}-O_{18}	-0.87569	31.53	68.47	0.5615	0.8275	$SP^{2.55}$	28.16	71.84
	1.96572							
O_{18}-H_{19}	-0.79201	76.16	23.84	0.8727	0.4882	$SP^{3.74}$	21.11	78.89

16. Fukui function

Fukui indices are, in short, reactivity indices they give us info concerning that atoms during a molecule have a large tendency to either loose or accept an electron, which we tend to chemist interpret as that are a

lot of susceptible to endure a nucleophilic or an electrophilic attack, respectively. The Fukui function is defined as [37].

$$f = \left(\frac{\delta\rho(r)}{\delta(N)}\right)r$$

where $\delta(r)$ is that the electronic density. N is the number of electrons and r is that the external potential exerted by the enzyme. Fukui Function (FF) is one of the wide useful local density functional descriptors to model chemical reactivity and selectivity. The Fukui Function may be a local reactivity descriptor that indicates the number of electron is modified. Therefore, it indicates the propensity of the electronic density to perform at a given position upon accepting or donating electrons [38, 39]. Also, it is possible to define the corresponding condensed or atomic Fukui Functions on the j^{th} atom site as,

$$f_j^+ = qj(N+1) - qj(N)$$

$$f_j^- = qj(N) - qj(N-1)$$

$$f_j^0 = \frac{1}{2}[qj(N+1) - qj(N-1)]$$

wherever f_j^+, f_j^-, f_j^0 are nucleophilic, electrophilic and free radical on the reference molecule, respectively. In these equations, q_j is that the atomic charge (evaluated from Mulliken population, electrostatic derived charge, etc.) at the j^{th} atomic site is the neutral (N), anionic (N+1) or (N-1) chemical species. Chattaraj et al. [40] have introduced the thought of generalized philicity. It contains the majority info concerning hitherto well-known completely different global and local reactivity and selectivity descriptor, in additionally to the data concerning electrophilic/nucleophilic power of a given atomic site during a molecule. Morell et al. [41] have recently planned a dual descriptor ($\Delta f(r)$), which is defined as the difference between the nucleophilic and electrophilic Fukui function and is given by the equation,

$$\Delta f(r) = [f^+(r) - f^-(r)]$$

$\Delta f(r)$>0, then the site is favored for a nucleophilic attack, whereas if $\Delta f(r)$<0, r then the site could also be favored for an electrophilic attack. According to dual descriptor $\Delta f(r)$ give a transparent distinction between nucleophilic and electrophilic attack at a particular site with their sign. That is they provide positive value prone for electrophilic attack. From the values reported in Table 9, according to the condition for dual descriptor, nucleophilic site for in our title molecule is C_1, C_4, C_5, C_6, C_8, C_{10}, H_{11}, O_{12}, C_{13}, H_{20}, H_{21}, H_{22}, H_{23}, H_{24} and H_{25} are Positive values i.e. $\Delta f(r)$>0). Similarly the electrophilic site is C_2, C_3, C_7, C_9, H_{14}, H_{15}, C_{16}, O_{17}, O_{18} and H_{19} Negative values i.e. $\Delta f(r)$<0). The behavior of molecule as electrophilic and nucleophilic attack throughout reaction depends on the local behavior of molecule.

Table 9

Using Mulliken population analysis: Fukui functions (f_k^+, f_k^-, f_k^0) for atoms of of Naphthalene-2-yloxy Acetic Acid at B3LYP/LANL2DZ and B3LYP/LANL2MB methods.

Atoms	Mulliken atomic charges			Fukui functions			
	$q_{(N+1)}$	qN_0	$q_{(N-1)}$	f_j^+	f_j^-	f_j^o	f (r)
C_1	-0.45771	-0.56910	-0.64125	0.11139	0.07215	0.18354	0.03924

C_2	0.45063	0.45398	0.44491	-0.00335	0.00907	0.00572	-0.01242
C_3	-0.28373	-0.22700	-0.24602	-0.05673	0.01902	-0.03771	-0.07575
C_4	-0.39707	-0.54053	-0.58322	0.14346	0.04269	0.18615	0.10077
C_5	-0.32273	-0.41220	-0.45715	0.08947	0.04495	0.13442	0.04452
C_6	-0.17462	-0.23033	-0.26041	0.05571	0.03008	0.08579	0.02563
C_7	-0.19224	-0.23353	-0.25910	0.04129	0.02557	0.06686	-0.00606
C_8	-0.31345	-0.39532	-0.44267	0.08187	0.04735	0.12922	0.03452
C_9	0.37557	0.38500	0.38987	-0.00943	-0.00487	-0.01430	-0.00456
C_{10}	0.39528	0.39687	0.40051	-0.00159	-0.00364	-0.00523	0.00205
H_{11}	0.29536	0.24576	0.21633	0.04960	0.02943	0.07903	0.02017
O_{12}	-0.21517	-0.26749	-0.29119	0.05232	0.02370	0.07602	0.02862
C_{13}	-0.28291	-0.36833	-0.39659	0.08542	0.02826	0.11368	0.05716
H_{14}	0.25487	0.23981	0.17833	0.01506	0.06148	0.07654	-0.04642
H_{15}	0.26979	0.28783	0.23984	-0.01804	0.04799	0.02992	-0.06603
C_{16}	0.20405	0.21310	0.03298	-0.00900	0.18012	0.17107	-0.18912
O_{17}	-0.22964	-0.19110	-0.35493	-0.03854	0.16383	0.12529	-0.20237
O_{18}	-0.43564	-0.40418	-0.43077	-0.03146	0.02659	-0.00487	-0.05805
H_{19}	0.41643	0.39210	0.34019	0.02433	0.05191	0.07624	-0.02758
H_{20}	0.28073	0.12009	0.15710	0.16064	-0.03701	0.12363	0.19765
H_{21}	0.27022	0.21808	0.19452	0.05214	0.02356	0.07570	0.02858
H_{22}	0.27319	0.22546	0.20255	0.04773	0.02291	0.07064	0.02482
H_{23}	0.27372	0.21670	0.18164	0.05636	0.03506	0.09208	0.02130
H_{24}	0.27282	0.21736	0.18194	0.05546	0.03542	0.09088	0.02004
H_{25}	0.27223	0.22698	0.20259	0.04525	0.02439	0.06964	0.02086

17. Molecular electrostatic potential (MEP)

Molecular electrostatic potential (MEP) is related to the electronic density and is a very helpful descriptor in understanding sites for electrophilic attack and nucleophilic reactions furthermore as hydrogen bonding interactions [42-44]. A predict reactive sites for electrophilic attack for the title compound. MEP was calculated at the B3LYP/LAL2DZ optimized geometry. For the systems studied the molecular electrostatic potential values were calculated

$$V(r) = \sum \frac{Z_A}{|R_A - r|} - \int \frac{\rho(r')}{|r' - r|} dr$$

wherever the summation runs over all the nuclei A in the compound and polarization and reorganization effects are neglected. Z_A is the charge of the nucleus A, located at R_A and $\rho(r')$ is the electron density function of the molecule. The molecular electrostatic potential countour maps for positive and negative sites of the title molecule NLA are shown in Fig. 11. The MEP plot of electrostatic potential is represented by completely different colors. Red represents the regions of the foremost negative electrostatic potential and blue represent the regions of the most positive electrostatic potential. Potential increases within the order red<orange<yellow<green<blue. The color grading of resulting surface simultaneously displays molecular size, shape and electrostatic potential value which are useful in research of molecular structure with its physiochemical property relationship [45]. As simply are over the electronegative atom (oxygen atom), the regions having the most positive potential are over the hydrogen

atoms. As can be seen from the MEP of the title molecule, more reactive sites are near C=O group, the region having the most negative potential over oxygen atom O_{17}. The negative potential value is -22.3892 a.u. indicates the strongest repulsion (electrophilic attack). A most positive region localized on the hydrogen atoms H13, H14, H11 and its values are 0.0953, 0.0977 and 0.0977 a.u. indicates the strongest attraction (nucleophilic attack), severally.

18. Hirshfeld surface analysis

Molecular Hirshfeld surfaces within the crystal structure are constructed basing on the electron distribution calculated as the sum of spherical atom electron densities (46, 47). Molecular Hirshfeld surfaces partition crystal space into smooth, non-overlapping, interlocking molecular volumes. Inside the Hirshfeld surface the electron distribution due to a sum of spherical atoms for the molecule (the pro-crystal) dominates the corresponding sum over the crystal (the pro-crystal), and the Hirshfeld surface is defined implicitly wherever the quantitative relation of pro-molecule to pro-crystal electron densities equals 0.5. As it depends intimately on the molecular geometry, the location and orientation of nearest and more distant neighboring molecules, and

Charge (e)	Atom	V(r) a.u
-0.5691	C1	-14.7497
0.453978	C2	-14.6839
-0.226995	C3	-14.7307
-0.540534	C4	-14.7493
-0.412198	C5	-14.7547
-0.230328	C6	-14.7541
-0.233532	C7	-14.7547
-0.39532	C8	-14.7547
ds0.385002	C9	-14.7431
0.396866	C10	-14.744
0.245756	H11	-1.08805
-0.267488	O12	-22.2995
-0.36833	C13	-14.6598
0.239812	H14	-1.04673
0.287827	H15	-1.05121
0.213096	C16	-14.5719
-0.191101	O17	-22.3057
-0.404181	O18	-22.2984
0.3921	H19	-0.89324
0.12009	H20	-1.05044
0.218075	H21	-1.08309
0.225456	H22	-1.09648
0.216703	H23	-1.1002
0.217363	H24	-1.10077
0.226982	H25	-1.09761

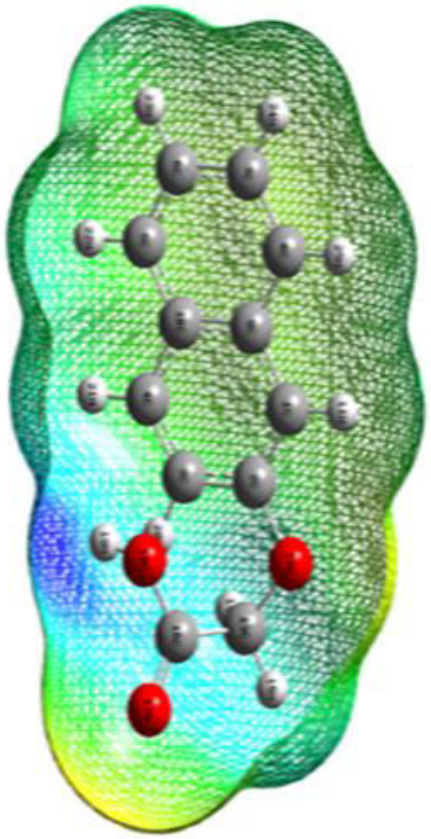

Fig. 11 Calculated 3D molecular electrostatic potential contour map for C8 conformer of NLA

the nature (radial extent) of specific atom types that build close contacts with the molecule in question, the Hirshfeld surface reflects in appreciable detail the immediate environment of a molecule during a crystal. For a given crystal structure and set of spherical atomic electron densities, the Hirshfeld surface is exclusive [48] and it is this property that implies the possibility of gaining further insight into the intermolecular interaction of molecular crystals. The Hirshfeld surface enclosure a molecule is defined by points wherever the contribution to the electron density from the molecule of interest is equal to the contribution from all the other molecules. For each point on that isosurface two distances are defined: d_e, the distance from the point to the nearest nucleus external to the surface, and d_i the distance to the nearest nucleus internal to the surface. The normalized contact distance (d_{norm}) based on both d_e and d_i, and the vdW radii of the atom, given by the equation

$$d_{norm} = d_i - ri^{vdW})/r_i^{vdW} + (de - r_e^{vdW})/r_e^{vdW}$$

enables identification of the regions of particular importance to intermolecular ineractions [49]. The value of the d_{norm} is negative or positive once intermolecular contacts are shorter/longer than vdW separation. Because of the symmetry between d_e and d_i in the expression for d_{norm}, where two Hirshfeld surfaces touch, can show a red spot identical in color intensity further as size and shape. The combination of d_e and d_i in the form of a 2D fingerprint plot provides outline of intermolecular contacts in the crystal [50]. The Hirshfeld surfaces are mapped with d_{norm} shape index; curvedness and 2D finger print plots given during this paper were generated using Crystal Explorer 2.1 [51]. The Hirshfeld surfaces of the title molecule illustrated in Fig.12 which shows surfaces that have been mapped over d_{norm} (-0.724 to 1.197 A°). It is clear that the information present in Table 10 is summarized effectively in these spots, with the massive circular depressions visible on the surfaces indicative of strong H-H interactions and therefore the blue color points in the two-dimensional fingerprint plots are indicative of short contacts for the C-C, C-O, C-H, H-O and O-O interactions. The H…H interactions have a lot of significant contribution to the total Hirshfeld surfaces of the title molecule, comprising 42.4 % and reflected in the middle of the scattered points in the two-dimensional fingerprint plot (d_i = 0.660 to 2.473 A° and d_e = 0.660 to 2.416 A°) as a blue color. The C…C interactions of the Hirshfeld surfaces of the title molecule 5.3 % , C…H is 20.2 , C…O is 5.3 % , O…H is 26.4 % and O…O is 0.4 % are shown in Fig. 11. The H…H interactions are still the main contribution to the whole Hirshfeld surfaces (42.4 %) and can be viewed as the "ridge" of the 2D finger print plots. The C…H interactions contribute 20.02 % to the total Hirshfeld surfaces and also are characterized as "wings" within the upper left and lower right regions of the 2D fingerprint plots.

19. Molecular docking studies

The prediction of molecular interactions between the lead molecule and targets (proteins, enzymes; etc.) of biological interest has become of great importance within the field of drug discovery. In additionally, by docking analysis of the lead molecule with many protein targets, one will simply realize insights into the underlying molecular mechanisms of selectivity [52]. In this work, both the rigid docking and partial blind docking approaches are used to find the activity of Naphthalene-2-yloxy acetic acid against the targets such as 4QOK(Medicago truncatula), 4PSB (Vigna radiate) and 4Y31(yellow lupine LlPR-10.1A) [53-54]. These plant growth proteins were elite on the idea of probability of binding given by the Swiss target prediction web interface [55]. The binding activities of Naphthalene-2-yloxy acetic acid with these targets haven't yet been disclosed. Docking studies of NLA have been done against plant growth proteins. The 3D crystal structure of this proteins were obtained from Protein Data Bank (PDB ID: 4QOK, 4PSB and 4Y31). Molecular docking was performed on Auto Dock Vina software package [56]. Auto Dock Tools (ADT) graphical computer programe was used to add polar hydrogens and to

calculate atomic charges by Kollman method. Water molecules and co-crystallized ligands were removed. NLA

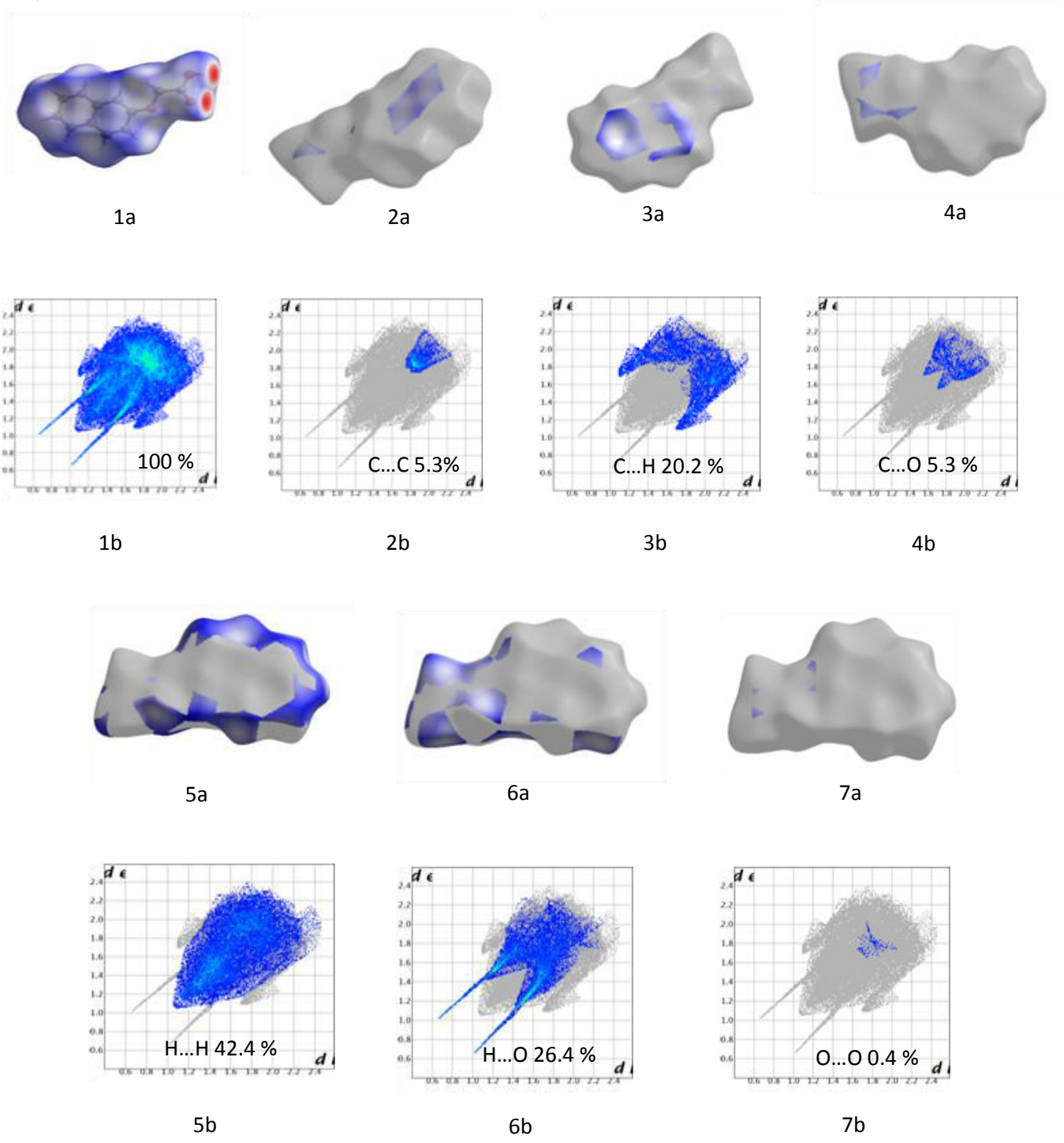

Fig. 12. Hirshfeld surface fingerprint plots of the nearest internal distance (di) vs the nearest external distance (de) for each of the crystallographically independent molecule in the Naphthalene-2-yloxy acetic acid. Each point on a HS can be represented by a coordinate (di,de). The colors represent the number of points with a given fingerprint plot coordinate (hot colors represent many points, cool colors represent few points). Picture a is structure contribution for Hirshfeld surfaces and b is fingerprint plots.

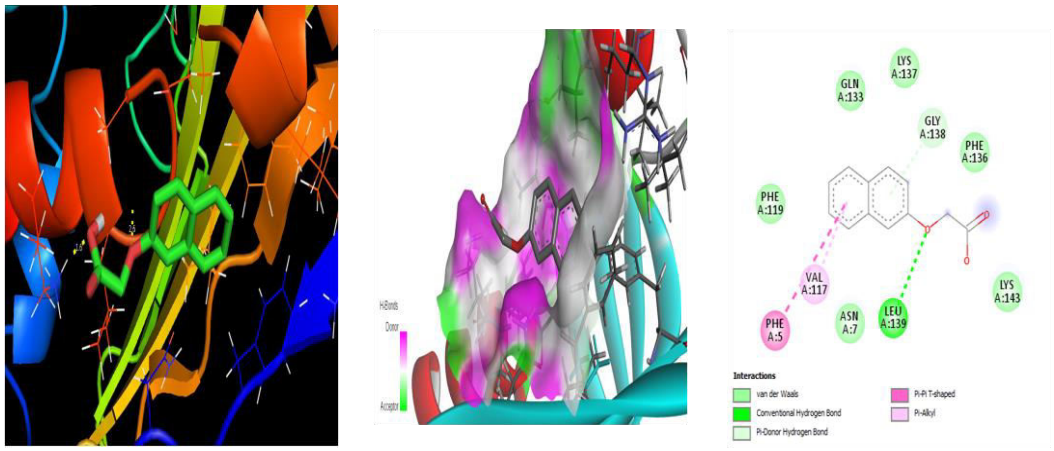

1a. 1b.

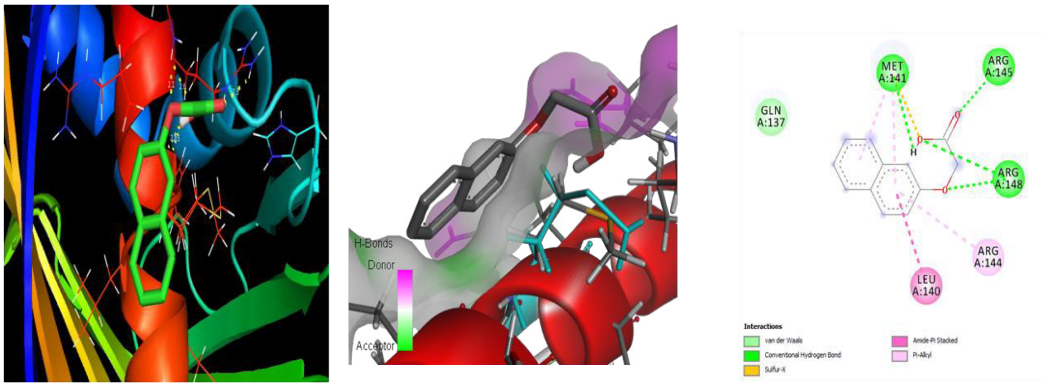

b. 4PSB

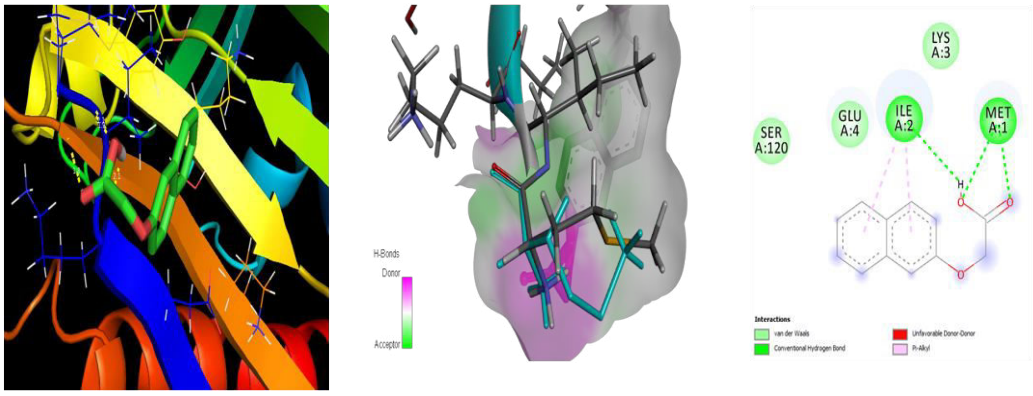

c. b.

Fig. 13 'a' and 'b' are Docking (4Y31, 4PSB and 4QOK) picture, 'c' 2D interaction for Naphthalene-2-yloxy acetic acid

was prepared for docking by minimizing its energy at B3LYP/ LANL2DZ level of theory. Partial charges were calculated by Geistenger method. Torsions and rotatable bonds were defined. The active site of the macromolecule was defined to incorporate residues of the active site within the grid size of 40 Å × 40 Å × 40 Å. To evaluate the quality of docking results, the common method is to calculate the Root Mean Square Deviation (RMSD) between the docked cause and therefore the well-known crystal structure conformation. RMSD values up to 2Å are considered reliable for a docking protocol [57]. Amongst the docked conformations of the co-crystallized ligand and scored well was visualized for ligand-protein interactions in Discovery Studio Visualizer 4.1 software.

The ligand binds at the active site of the macromolecule (protein) by weak covalent interactions most distinguished of that are H-bonding interactions Figs. 13 a-c. Table 11 denote the most effective Binding free energy (ΔG) of -6.70 kcal/mol as predicted by Auto Dock Vina suggests good binding affinity.

20. **Conclusion**

FT-IR and FT-Raman spectra of Naphthalen-2-yloxy acetic acid were studied experimentally and theoretically. The molecular geometry and wavenumbers were calculated using DFT method and the optimized geometrical parameters. The stability of the molecule arising from hyper-conjugative interaction and charge delocalization has been analyzed using NBO analysis. The HOMO, LUMO, DOS and OPDOS analysis are used to determine the charge transfer within the molecule. MEP was performed by DFT method. The dipole moment, polarizability and hyperpolarizability values are predicted. The Fukui functions showed that the ring and substitution atoms are the most probable sites for electrophilic and nucleophilic attacks. The Hirshfeld surface and fingerprint plot analysis, which act as a novel method of visualizing the intermolecular interactions, show that the close contacts of NLA in the title molecule dominated by the C-C, C-H, C-O, H-H, H-O and O-O interactions. These interactions play a key role towards the stabilization of the molecule in the solid state and these interactions also have prominent signatures in the finger plots. The binding activity of NLA with biological targets of interest was examined by docking analysis and discussed in terms of interaction energy calculated by ADV.

References

[1] Baldwin, C.R., M.M. Britton, S.C. Davies, D.G. Gillies, D.L. Hughes, G.W. Smith and L.H. Sutcliffe, X-ray crystallography and NMR spectroscopy of some cyclohexyl esters. J. Mol. Str. 403 (1997) 1-16.

[2] Agency for Toxic substances Disease Registry (ASTR), Department of Health and Human Services, Public services.

[3] Frisch, M.J., G.W. Trucks, H.B. Schkegel, G.C. Scuseria, M.A. Robb, J.R. Cheeseman, G. Scalmani, V. Barone, B. Mennucci, G.A. Bloino, G. Zheng, J.L Sonnenberg, M. Hada, M. Ehara, K.Toyota, R. Fkuda, J. Hasegawa, M. Ishida, T. Nakajima, Y. Honda, O. Kitao, H. Nakai, T.vreven, J.A. Montgomery, J.E. Peralta, F. Ogliaro, M. Bearpark, J.J. Heyd, E. Brothers, K.N. Kudin, V.N. Staroverov, T. Keith, R. Kobayashi, J. Normand, K.Rghavachri, A.Rendell, J.C. Burant, S.S. Iyengar, J. Tomasi, M.Cossi, N. Rega, J.M. Millam, M. Klene,

J.E. Knox, J.B. Cross, V. Bakken, C. Adamo, J.Jaramillo, R. Gomperts, R.E. Stratmann, O. Yazyev, A.J. Austin, R. Cammi, C. Pomelli, J.W. Ochterski, R.L. Martin, K. Morokuma, V.G. Zakrzewski, G.A. Voth, P. Salvador, J.J. Dannenberg, S. Dapprich, A.D. Daniels, O. Farkas, J.B. Foresman, J.V. Ortiz, J. Cioslowski, D.J. Fox, Gaussian Inc, Wallingford CT, 2010.

[4] Foresman, J.B., in:E. Frisch (Ed.), Exploring Chemistry with Electronic Structure methods: A Guide to using Gaussian, Pittsburg, PA, 1996.

[5] Dennington, R., T. Keith, J. Millam, Gaussview, Version 5, Semichem Inc., Shawnee Mission KS,2009.

[6] Vijakumar, S., L.M. Rao, Acta Crystallogr. (4-Chlorophenoxy) acetic acid. B 38 (1982) 2062–2064.

[7] Polavarapu, P.L., Ab initio vibrational Raman and Raman optical activity spectra J. Phys. Chem. 94 (1990) 8106–8112.

[8] Keresztury, G., S. Holly, J. Varga, G. Besenyei, A.Y.Wang, J.R. Durig, Vibrational spectra of monothiocarbamates-II. IR and Raman spectra, vibrational assignment, conformational analysis and *ab initio* calculations of *S*-methyl-*N,N*-dimethylthiocarbamate. Spectrochim. Acta 49A (1993) 2007–2026.

[9] Sundius, T., J. Mol. Struct. Molvib - A flexible program for force field calculations 218 (1990) 321–326.

[10] Bellamy, L.J., The Infrared Spectra of Complex Molecules, third ed., Wiley, New 642 York, 1975.

[11] Varsanyi, G., Assignments for Vibrational Spectra of Seven Hundred Benzene Derivatives, vol. I, Adam Hilger, London, 1974.

[12] Smith, B., Infrared Spectral interpretation, A systematic approach, CRC: Washington, DC, 1999

[13] Mohan, J., Organic spectroscopy – Principles and applications (2nd edn), Narosa publishing House: New Delhi, 2001.

[14] Bellamy, L.J., The Infrared Spectra of Complex Molecules, third ed., Wiley, New York, 1975.

[15] Varsanyi, G., Assignments for Vibrational Spectra of Seven Hundred Benzene Derivatives, vol. I, Adam Hilger, London, 1974.

[16] George, W.O., P.S. Cintyne, in Infrared Spectroscopy (Ed.: D.J. Mowthrope), John Willey and Sons: UK, 1987.

[17] Sathyanarayana, D.N., Vibrational Spectroscopy – Theory and Applications (2nd edn), New Age International (P) Limited Publishers: New Delhi, 2004.

[18] Vein, D.L., N.B. Colthup, W.G. Fateley, J.G. Grasselli, The Handbook of Infrared and Raman Characteristic Frequencies of Organic Molecules, Academic Press, San Diego, 1991.

[19] Andraud, C., T. Brotin, C. Garcia, F. Pelle, P. Goldner, B. Bigot, A. Collet, Theoretical and experimental investigations of the nonlinear optical properties of vanillin, polyenovanillin, and bisvanillin derivatives. J. Am. Chem. Soc. 116 (1994) 2094-2102.

[20] Karabacak, M., A.M. Asiri, A.O. Al-Youbi, A.H. Qusti, M. Clinar, Identification of structural and spectral features of synthesized cyano-stilbene dye derivatives: A comparative experimental and DFT study Spectrochim. Acta A 120 (2014) 144-150.

[21] O'Boyle, N.M., A.L. Tenderholt, K.M. Langner, cclib: A library for package-independent computational chemistry algorithms. J. Comp. Chem. 29 (2008) 839–845.

[22] Hoffmann, R., Solids and Surfaces: A Chemist's View of Bonding in Extended Structures, VCH Publishers, New York, 1988.

[23] Hughbanks, T., R. Hoffmann, Chains of trans-edge-sharing molybdenum octahedra: metal-metal bonding in extended systems J. Am. Chem. Soc. 105 (1983) 3528-3537.

[24] Małecki, J.G., Synthesis, crystal, molecular and electronic structures of thiocyanate ruthenium complexes with pyridine and its derivatives as ligands, Polyhedron 29 (2010) 1973-1979.

[25] Chen, M., U.V. Waghmare, C.M. Friend, E. Kaxiras, A density functional study of clean and hydrogen-covered α-MoO3(010):α-MoO3(010): Electronic structure and surface relaxation, J. Chem. Phys. 109 (1998) 6654-6660.

[26] Zhang, R., B. Dub, G. Sun, Y. Sun, Experimental and theoretical studies on o-, m- and p-chlorobenzylideneaminoantipyrines, Spectrohim. Acta A 75 (2010) 1115-1124.

[27] Balachandran, V., A. Nataraj, T. Karthick, M. Karabacak, A. Atac, FT-Raman, FT-IR, UV spectra and DFT and ab initio calculations on monomeric and dimeric structures of 3,5-pyridinedicarboxylic acid J. Mol. Struct. 1027 (2012) 1-14.

[28] Chemia, D.S., J. Zyss, Non Linear Optical Properties of Organic Molecules and Crystal, Academic Press, New York. 1987.

[29] Zyss, J., Molecular Non Linear Optics, Academic Press, Boston. 1994.

[30] Karabacak, M., L. Sinha, O. Prasad, A.M. Asiri, M. Cinar, An experimental and theoretical investigation of Acenaphthene-5-boronic acid: Conformational study, NBO and NLO analysis, molecular structure and FT-IR, FT-Raman, NMR and UV spectra, Spectrochim. Acta A115 (2013) 753-766.

[31] Sajan, D., T.U. Devi, K. Safakath, R. Philip, I. Nemec, M. Karabacak, Ultrafast optical nonlinearity, electronic absorption, vibrational spectra and solvent effect studies of ninhydrin, Spectrochim. Acta A 109 (2013) 331-349.

[32] Amila, K., K.M. Jeewandara, S. de Nalin, Are donor–acceptor self organised aromatic systems NLO (non-linear optical) active? J. Mol. Structure Theochem. 686 (2004) 131-136.

[33] Sundaraganesan, N., J. Karpagam, S. Sebastian, J.p. Cornard, The spectroscopic (FTIR, FT-IR gas phase and FT-Raman), first order hyperpolarizabilities, NMR analysis of 2,4-dichloroaniline by ab initio HF and density functional methods, Spectrochim Acta A 73 (2009) 11-19.

[34] Szafran, M., A. Komasa, E.B. Adamska, Crystal and molecular structure of 4-carboxypiperidinium chloride (4-poperidinecarboxylic acid hydrochloride), J. Mol. Struct. (Theochem.) 827 (2007) 101-107.

[35] Silverstein, M., X. Webster, G. Basseter, C. Morill, Spectrometric Identification of Organic Compounds, Wiley, New York, 1981.

[36] Parr, R.G., W. Yang, Functional Theory of Atoms and Molecule, Oxford University Press, New York, 1989.

[37] Ayers, P.W., R.G. Parr, Variational Principles for Describing Chemical Reactions: The Fukui Function and Chemical Hardness Revisited, J. Am. Chem. Soc. 122 (2000) 2010-2018.

[38] Parr R. G., amd W. Uang.Density functional approach to the frontier-electron theory of chemical reactivity, J. Am. Chem. Soc. 106 (1984) 4049-4050.

[39] Chattaraj, P.K., B. Maiti, U. Sarkar, Philicity: A Unified Treatment of Chemical Reactivity and Selectivity, J. Phys. Chem. A 107 (2003) 4973–4975.

[40] Morell, C., A. Grand, A. Toro-Labbe, New Dual Descriptor for Chemical Reactivity, J. Phys. Chem. A 109 (2005) 205–212.

[41] Scroco, E., J. Tomasi, Adv, Electronic Molecular Structure, Reactivity and Intermolecular Forces: An Euristic Interpretation by Means of Electrostatic Molecular Potentials, Quantum chem. 11 (1979) 115-193.

[42] Luque, F.F., J.M. Lopez, M. Orozco, Perspective on "Electrostatic interactions of a solute with a continuum. A direct utilization of ab initio molecular potentials for the prevision of solvent effects", Theor. Chem. Acc. 103 (2000), 343-345.

[43] Qkulik, N., A.H. Jubert, Theoretical Analysis of the Reactive Sites of Non–steroidal Anti–inflammatory Drugs, J. Mol. Des. 4 (2005), 17-30.

[44] Szafram. M., A. Komasa, E.B. Adamska, Crystal and molecular structure of 4-carboxypiperidinium chloride (4-piperidinecarboxylic acid hydrochloride), J. Mol. Structure (Theochem.) 827 (2007) 101-107.

[45] Spackman M.A., and P. G. Byrom, A novel definition of a molecule in a crystal, Chem.Phys. Lett. 267 (1997) 215–220.

[46] McKinnon, J. J., A. S. Mitchell and M. A. Spackman, Hirshfeld Surfaces: A New Tool for Visualizing and Exploring Molecular Crystals, Chem.–Eur. J. 4 (1998) 2136–2141.

[47] McKinnon, J. J., M. A. Spackman and A. S. Mitchell, Acta Crystallogr., Novel tools for visualizing and exploring intermolecular interactions in molecular crystals, Sect. B: Struct. Sci., 60 (2004) 627–668.

[48] Kepert, C. J., Advanced functional properties in nanoporous coordination framework materials. Chem. Commun., 7 (2006) 695–700.

[49] Spackman M. A. and J. J. McKinnon, Fingerprinting intermolecular interactions in molecular crystals CrystEngComm, 4 (2002) 378–392.

[50] Cai J, Han C, Hu T, Zhang J,Wu D,Wang F, Liu Y, Ding J, Chen K,Yue J, Shen X, Jiang H (2006) Peptide deformylase is a potential target for anti-helicobacter pylori drugs: reverse docking, enzymaticassay, and X-ray crystallography validation. Protein Sci 15:2071–2081.

[51] Gfeller D, Grosdidier A, Zoete V (2014) Swiss target prediction: a web server for target prediction of bioactive small molecules. Nucl. Acids Res 42(W1):W32–W38.

[52] Milosz Ruszkowski, Joanna Sliwiak, Agnieszk Ciesielska, Jakub Barciszewski, Michal Sikorskia and Mariusz, Jaskolskia., Specific binding of gibberellic acid by CytokininSpecific Binding Proteins: a new aspect of plant hormone-binding proteins with the PR-10 fold, Acta Cryst. D70 (2014). 2032–2041.

[53] Joanna S liwiak , Rafał Dolot , Karolina Michalska, Kamil Szpotkowski, Grzegorz Bujacz,Michał Sikorski , Mariusz Jaskolski, Crystallographic and CD probing of ligand-induced conformational changes in a plant PR-10 protein, J. Structural Bio.193 (2016) 55–66.

[54] Gfeller D, Michielin O, Zoete V (2013) Shaping the interaction landscape of bioactive molecules. Bioinformatics 29 (2013) 3073–3079.

[55] Trott, O., Olson, A.J., 2010. Software news and update Auto Dock Vina: Improving the speed and accuracy of docking with a new scoring function, efficient optimization, and multithreading, J. Comput. Chem. 31 (2010) 455-461.

[56] Kramer, B., Rarey, M., Lengauer, T., Evaluation of the FLEXX incremental construction algorithm for protein–ligand docking, Proteins 37 (1999) 228-241.